

A Close Look at Mechanism, Application, and Opportunities of Electrochemiluminescence Microscopy

Xiaodan Gou, Zejing Xing, Cheng Ma,* and Jun-Jie Zhu*

Cite This: *Chem. Biomed. Imaging* 2023, 1, 414–433

Read Online

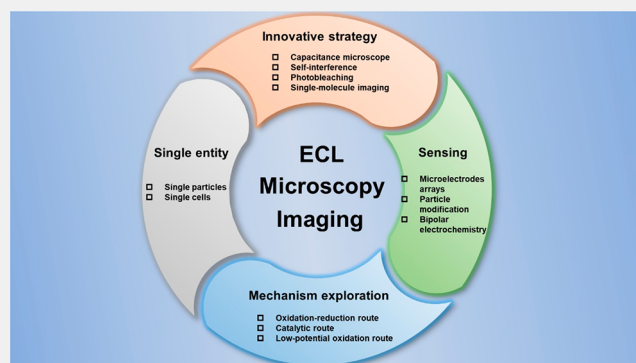
ACCESS |

Metrics & More

Article Recommendations

ABSTRACT: Electrochemiluminescence (ECL) is a typical luminescence process triggered by electrochemical reactions. Due to the separated signal types, ECL measurements have some merits of high sensitivity, low background, and simple configuration. Coupled with a microscopy setup, ECL microscopy (ECLM) has the unique characteristics of ECL and is also furnished with spatiotemporal resolution. Thus, many applications have been created, including nanoscale sensing, ECL mechanism deciphering, transient events of single objects, and ECLM crossover methods. In this review, we will overview the development and basic knowledge of ECL and then profile the setup design of ECLM. Through the understanding of these two parts, we will next probe the diverse applications of ECLM, combining the inter-relation with each other. Finally, the outlook discussing the expectations of further progress of ECLM technology.

KEYWORDS: *Electrochemiluminescence, Microscopy, Sensing, Mechanism exploration, Single entity, Single cell, Spatiotemporal resolution, Bipolar electrode*



1. INTRODUCTION

The emergence of optical microscopy imaging is destined to become a revolutionary technique, showing a new world of microscale in various fields. Recent years have witnessed a significant increase of many different optical microscopies widely applied in chemical, biological, and medical areas, due to their common strengths of visualization as well as noninvasion ability. Nevertheless, a significant problem is that an applied light source is necessary for most usual optical imaging methods, decreasing imaging sensitivity and somehow triggering the photobleaching as well as phototoxic damage,^{1,2} which limits the development of optical imaging techniques to a large extent.

Electrochemiluminescence (ECL) is a kind of light emission process generated by electron transfer reactions between electrochemically produced intermediates without excitation light.³ With the combination of optical and electrochemical methods, it represents many advantages such as a wide dynamic range, excellent spatiotemporal controllability, and high sensitivity,^{4,5} bringing ECL from a basic investigation to various practical applications including detection of small molecules,^{6,7} nucleic acids,^{8–10} as well as proteins^{11,12} and cells^{13,14} or bacteria^{15,16} sensing. In particular, ECL-based immunoassays show high commercial values and have even become the gold standard in clinical diagnosis.⁵ Subsequently, ECL has drawn attention in the field of optical imaging

because it can overcome the limitations imposed by external light. Thus, traditional photomultiplier tubes (PMTs) are replaced by a camera with two-dimensional array optical units,¹⁷ making ECL a novel optical microscopy imaging strategy with low background and high spatiotemporal resolution. These advantages benefit high-throughput sensing and single-cell or particle research. Additionally, the most unique feature of this imaging method is surface sensitivity because light emission is confined in the vicinity of the electrodes,¹⁸ which is later utilized to investigate single-particle collision^{19,20} and cell–matrix adhesion²¹ and even the subcellular structure.²²

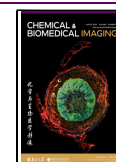
However, compared with fluorescence microscopy imaging, the development of ECL microscopy (ECLM) is relatively slow. Challenges as well as opportunities need to be addressed, including the low emission efficiency, an unclear mechanism, and biotoxicity. In recent years, as researchers continue to explore and improve the technique, these problems have been solved to some extent. By adapting single-photon counter

Received: December 19, 2022

Revised: January 29, 2023

Accepted: February 7, 2023

Published: March 6, 2023



- Aggregation-induced ECL**
S. Carrara, A. Allprandi, C. F. Hogan, L. De Cola.
J. Am. Chem. Soc. **2017**, 139, 14605
- ECL from single nanoparticles**
Y.-L. Chang, R. E. Palacios, F.-R. F. Fan, A. J. Bard, P. F. Barbara.
J. Am. Chem. Soc. **2008**, 130, 8906
- ECL from nanocrystal quantum dots**
Z. Ding, B. M. Quinn, S. K. Haram, L. E. Pell, B. A. Korgel, A. J. Bard.
Science **2002**, 296, 1293
- Bipolar ECL**
A. Arora, J. C. T. Eijkel, W. E. Morf, A. Manz.
Anal. Chem. **2001**, 73, 3282
- ECL from single molecules in solution**
M. M. Collinson, R. M. Wightman.
Science **1995**, 268, 1883
- ECL at ultramicroelectrodes**
M. M. Collinson, R. M. Wightman.
Anal. Chem. **1993**, 65, 2576
- TPRA as coreactant**
J. K. Leland, M. J. Powell.
J. Electrochem. Soc. **1990**, 137, 312
- [Ru(bpy)₃]²⁺ in polymer films**
I. Rubinstein, A. J. Bard.
J. Am. Chem. Soc. **1981**, 103, 5007
- Oxalate as coreactant**
M.-M. Chang, T. Saji, A. J. Bard.
J. Am. Chem. Soc. **1977**, 99, 5399
- Theory of ECL transients**
S. W. Feldberg.
J. Am. Chem. Soc. **1966**, 88, 390
- ECL of aromatic hydrocarbons**
D. M. Hercules.
Science **1964**, 145, 808
- R. E. Visco, E. A. Chandross.
J. Am. Chem. Soc. **1964**, 86, 5350
- K. S. V. Santhanam, A. J. Bard.
J. Am. Chem. Soc. **1965**, 87, 139
- ECL microscopy of cells**
S. Voci, B. Goudeau, G. Valentini, A. Lesch, M. Jovic, S. Rapino, F. Paolucci, S. Arbault, N. Sojic.
J. Am. Chem. Soc. **2018**, 140, 14753
- 3D ECL**
M. Sentic, S. Arbault, L. Bouffier, D. Manojlovic, A. Kuhn, N. Sojic.
Chem. Sci. **2015**, 6, 4433
- 2-(dibutylamino)ethanol as an efficient coreactant**
X. Liu, L. Shi, W. Niu, H. Li, G. Xu.
Angew. Chem. Int. Ed. **2007**, 46, 421
- Near-field scanning ECL microscopy**
Y. Zu, Z. Ding, J. Zhou, Y. Lee, A. J. Bard.
Anal. Chem. **2001**, 73, 2153
- Laser-action driven by ECL**
T. Horiuchi, O. Niwa, N. Hatakenaka.
Nature **1998**, 394, 659
- 1994: First commercial ECL instrument for bioassays by Igen International, Inc.**
- Bioassays**
G. F. Blackburn *et al.*
Clin. Chem. **1991**, 37, 1534
- A. J. Bard, G. M. Whitesides.
U.S. Patent **5,1993**, 221,605
- Persulfate as coreactant**
H. S. White, A. J. Bard.
J. Am. Chem. Soc. **1982**, 104, 6891
- Aqueous coreactant**
I. Rubinstein, A. J. Bard.
J. Am. Chem. Soc. **1981**, 103, 512
- [Ru(bpy)₃]²⁺**
N. E. Tokel, A. J. Bard.
J. Am. Chem. Soc. **1972**, 94, 2862
- Effects of magnetic fields**
L. R. Faulkner, A. J. Bard.
J. Am. Chem. Soc. **1969**, 91, 209
- Theory of CL/ECL electron-transfer-reactions**
R. A. Marcus.
J. Chem. Phys. **1965**, 43, 2654
- Luminescence during electrolysis of Grignard compounds and luminol**
Dufford, R. T.; Nightingale, D.; Gaddum, L. W., Jr.
J. Am. Chem. Soc. **1927**, 49, 1858
- Harvey, N., *J. Phys. Chem.* **1929**, 33, 1456

Figure 1. Development history of ECL from 1929 to 2018. Reprinted with permission from ref 28. Copyright 2019 Royal Society of Chemistry.

devices, outstanding cameras such as electron-multiplying charge-coupled device (EMCCD), and objectives with higher numerical apertures, the collection efficiency of weak luminescence can be enhanced,²³ enabling single-molecule ECL imaging.²⁴ Due to the excellent axial resolution of imaging techniques, the change of the ECL layer thickness can be directly observed,²⁵ which allows researchers to better understand the mechanism of luminescence. With the appearance of novel ECL reaction systems, some low or nontoxic reagents are used in biological imaging, and the dynamic ECLM imaging of single cells is realized.²¹ As a result, the application of ECLM can be further extended. In this review, we first introduce the development, main mechanisms, along with some common reaction systems of ECL. Then, after briefly describing the setup of ECLM, we will summarize and discuss its applications in detail, providing outlook for the future development of this technique.

2. DEVELOPMENT OF ECL

The history of ECL can be traced back to 1929 when Harvey discovered the luminescence of aminophthalichydrazid in the process of an electrochemical reaction and termed this phenomenon as galvano-luminescence.²⁶ Hercules then observed chemiluminescence during electrolysis of aromatic hydrocarbons at the cathode and discussed its possible mechanism in 1964, which can be seen as the first detailed report about ECL.²⁷ After that, ECL received wide attention and inspired researchers to deeply study this phenomenon and the underlying mechanism, further promoting its rapid development (Figure 1). Among various ECL-related chemical reaction systems, the most representative one is tris(2,2'-pyridine) ruthenium(II) (Ru(bpy)₃²⁺). Following about 60

years of study, ECL has become an excellent analytical technique and is widely applied in many areas such as food and water testing, immunoassays, and biosensing.²⁸

3. MECHANISMS OF ECL

As mentioned before, ECL is caused by the reactions between electrode species. Thus, according to different reaction mechanisms, it can be divided into two dominant categories, namely, the annihilation pathway and the co-reactant pathway.

3.1. Annihilation Pathway

Annihilation ECL was initially discovered and investigated. The process of this pathway can be shortly described as follows: the emitter (R) can be oxidized to form radical cation (R^{•+}) and reduced to form radical anion (R^{•-}) by applying step potential at a working electrode, and then both of them are annihilated via an exergonic electron transfer reaction to produce the excited state of the emitter (R*) which will later relax to the ground state by emitting luminescence.

It is worth noting that the generated excited species can be either the singlet state (¹R*) or the triplet state (³R*), depending on the available excitation energy within the exergonic electron transfer reaction. For moderate exergonic processes, the so-called “T route” dominates, where ³R* is mainly generated.²⁹ A representative example of luminophores through this mechanism is DPA (DPA = 9,10-diphenylanthracene). For strong exergonic processes, the emission pathway named the “S route” will occur,³⁰ where ¹R* can be directly generated, followed by most aromatic compounds. There is another process named the “E route”, where the exothermicity of the reactions is too small to excite R but could

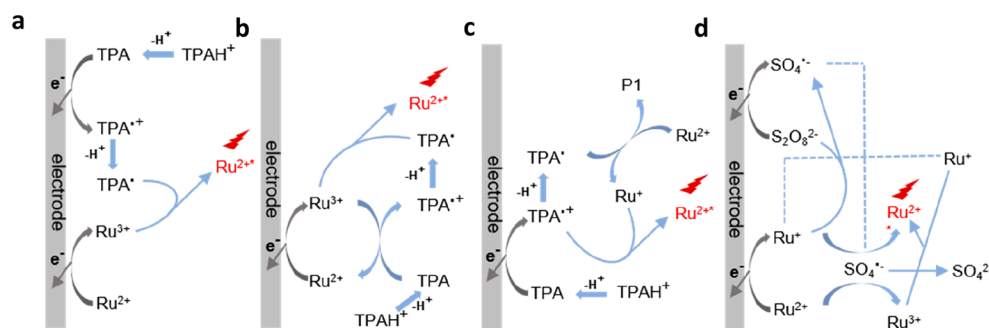


Figure 2. Mechanism of $\text{Ru}(\text{bpy})_3^{2+}/\text{TPA}$ (a–c) and $\text{Ru}(\text{bpy})_3^{2+}/\text{K}_2\text{S}_2\text{O}_8$ (d) ECL systems. Three different reaction routes in $\text{Ru}(\text{bpy})_3^{2+}/\text{TPA}$ ECL system: oxidative–reduction route (a), catalytic route (b), and low-potential oxidation route (c). In this figure, Ru^+ , Ru^{2+} , Ru^{3+} , and Ru^{2+*} denote $\text{Ru}(\text{bpy})_3^+$, $\text{Ru}(\text{bpy})_3^{2+}$, $\text{Ru}(\text{bpy})_3^{3+}$, and $\text{Ru}(\text{bpy})_3^{2+*}$, respectively; TPAH^+ , TPA , TPA^{*+} , and TPA^\bullet denote protonation of tri-*n*-propylamine, tri-*n*-propylamine, cationic radical of tri-*n*-propylamine, and radical of tri-*n*-propylamine, respectively; P1 is the oxidative production of the tri-*n*-propylamine radical.

still collect the light emission, often being ignored in most situations.³¹

3.2. Co-reactant Pathway

In 1977, Bard found that the simultaneous electrochemical oxidation of oxalate and luminophores could trigger light emission, which was the first report of co-reactants being involved in ECL generation.³²

The co-reactant pathway can be described as follows. First, the co-reactant is initially electrochemically oxidized or reduced to a radical intermediate. Then it converts to a strong reducing or oxidizing species to react with oxidized or reduced luminophores in the vicinity of the electrode. Last, the excited states could be generated via an electron transfer process to emit light. Different from the annihilation pathway, the ECL by the co-reactant pathway can be produced through only one-directional potential scanning on working electrodes due to the existence of co-reactants in solutions.

Based on the different redox abilities of species, it can be divided into two types: the “oxidative–reduction route” and the “reductive–oxidation route”. The former type represents the situation in which the generation of ECL was from a strong reducing species after electrochemical oxidation of co-reactants, where the classic co-reactants include oxalate,³³ cerium(III) sulfate,³⁴ and tri-*n*-propylamine (TPA). In contrast, the latter one refers to the situation in which the ECL generation was caused by strong oxidizing intermediates from electrochemical reducing products of co-reactants, where the representative co-reactants are benzoyl peroxide (BPO),³⁵ hydrazine,³⁶ and potassium persulfate ($\text{K}_2\text{S}_2\text{O}_8$).

4. SYSTEMS OF ECL

There are many chemical systems that can cause the ECL phenomenon. According to the difference of luminophores, these systems can be divided into three categories involving inorganic systems, organic systems, and nanomaterial-based systems. Among them, $\text{Ru}(\text{bpy})_3^{2+}$ and luminol are the most typical luminophores in inorganic and organic ECL systems, respectively. This section mainly discusses these two luminophores and will also add some common nanomaterial-based ECL systems.

4.1. $\text{Ru}(\text{bpy})_3^{2+}$ -Based System

$\text{Ru}(\text{bpy})_3^{2+}$ and its derivatives have been widely employed in various fields such as dye-sensitized solar cells, organic light-emitting diodes (OLED), photodynamic therapy (PDT), as

well as photocatalysis due to their excellent photochemical properties.³⁷ In 1972, Bard first observed that $\text{Ru}(\text{bpy})_3^{2+}$ in acetonitrile solution could generate ECL,³⁸ which was a landmark discovery in the field of ECL. From then on, researchers started to explore the $\text{Ru}(\text{bpy})_3^{2+}$ -based ECL systems, where the most commonly used co-reactant is TPA.

There are three possible reaction routes in this typical ECL system with $\text{Ru}(\text{bpy})_3^{2+}$ as luminophores and TPA as co-reactants. First, as shown in Figure 2a, the “oxidative–reduction route” could be summarized as follows: $\text{Ru}(\text{bpy})_3^{2+}$ and TPA are simultaneously electrochemically oxidized into $\text{Ru}(\text{bpy})_3^{3+}$ and TPA^{*+} , and then TPA^{*+} converts to a strong reducing radical intermediate TPA^\bullet by losing a proton, which can later reduce $\text{Ru}(\text{bpy})_3^{3+}$ to $\text{Ru}(\text{bpy})_3^{2+*}$ and lead to light emission.³³ It is worth noting that this route is the most representative and common one with very bright ECL generation.

After that, another mechanism named the “catalytic route” was discovered, as shown in Figure 2b. The main difference between these two routes is the heterogeneous or homogeneous oxidation process of TPA. In the “catalytic route”, TPA is oxidized by $\text{Ru}(\text{bpy})_3^{3+}$ rather than by an anodic electrode, followed by the same rest process as that in the “oxidation–reduction route”.³⁹ The “catalytic route” will be predominant when the concentration of TPA is relatively low, thus obtaining a thicker ECL layer (TEL) due to the long lifetime of adequate $\text{Ru}(\text{bpy})_3^{3+}$.⁴⁰

Additionally, the ECL emission can also be collected surprisingly when the applied potential is not high enough to trigger the oxidation of $\text{Ru}(\text{bpy})_3^{2+}$ but could still oxidize TPA. Therefore, a novel route has been confirmed, called the “low-oxidation potential (LOP) route” (Figure 2c). In this route, only TPA is oxidized on the working electrode, producing strong reducing TPA^\bullet which converts $\text{Ru}(\text{bpy})_3^{2+}$ to $\text{Ru}(\text{bpy})_3^+$. Subsequently, $\text{Ru}(\text{bpy})_3^+$ is again oxidized to $\text{Ru}(\text{bpy})_3^{2+*}$ by TPA^{*+} to emit light.⁴¹ Besides the above mentioned condition, there is another condition usually in the sensing applications in which $\text{Ru}(\text{bpy})_3^{2+}$ is immobilized on objects (such as microbeads or cells) and cannot directly participate in the electrochemical reaction, allowing ECL to generate by the electrochemical oxidation of TPA.

As people continuously research co-reactants, some other amines were found to be functionally identical as TPA within $\text{Ru}(\text{bpy})_3^{2+}$ -based ECL systems, such as 2-(dibutylamino)-ethanol (DBAE)⁴² and *N*-(2-hydroxyethyl)piperazine-*N'*-(2-

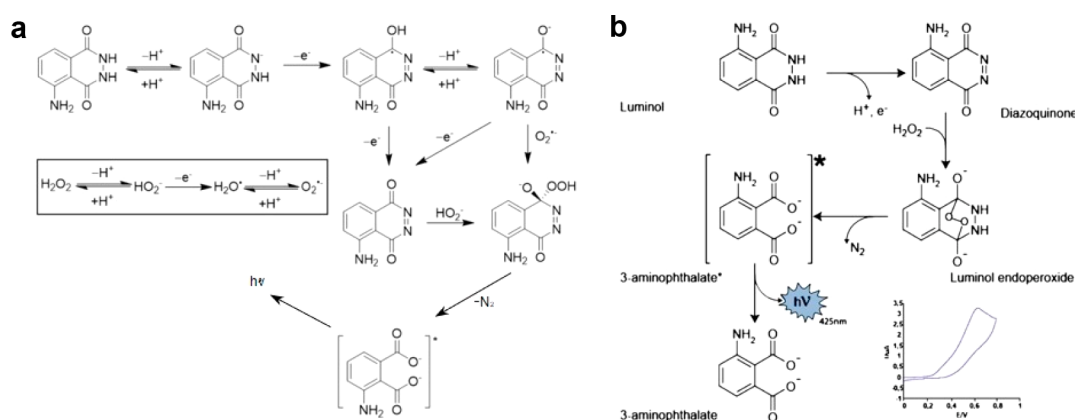


Figure 3. Mechanism of the luminol/ H_2O_2 ECL system. H_2O_2 acts as both co-reactant and oxidant in the ECL reaction (a) and only acts as an oxidant in the ECL reaction (b). Reprinted with permission from ref 49 (copyright 2022 Wiley-VCH) and ref 50 (copyright 2020 Wiley-VCH).

ethane sulfonic acid) (HEPES).⁴³ Meanwhile, these co-reactants have their own advantages, somehow compensating the limitations of TPA. For example, DBAE can catalyze the direct oxidation of amines with the help of its hydroxyethyl group, thus enhancing the ECL efficiency.⁴² HEPES has excellent biocompatibility and is more suitable for the investigation on living cells.⁴³

Notice that, in the absence of co-reactants, the $\text{Ru}(\text{bpy})_3^{2+}$ -based ECL can also be generated under the annihilation pathway. Briefly, $\text{Ru}(\text{bpy})_3^{2+}$ can be oxidized to $\text{Ru}(\text{bpy})_3^{3+}$ and reduced to $\text{Ru}(\text{bpy})_3^+$ by applying a step potential, then both of them are annihilated to the excited state of $\text{Ru}(\text{bpy})_3^{2+}$ ($\text{Ru}(\text{bpy})_3^{2+*}$) which will later relax to the ground state and generate luminescence.

There is another kind of co-reactant that can trigger the ECL generation of $\text{Ru}(\text{bpy})_3^{2+}$ through the reductive–oxidation mechanism, here taking potassium persulfate ($\text{K}_2\text{S}_2\text{O}_8$) as an example (Figure 2d). In this system, $\text{S}_2\text{O}_8^{2-}$ and $\text{Ru}(\text{bpy})_3^{2+}$ are simultaneously electrochemically reduced to strong oxidizing radical intermediates $\text{SO}_4^{\cdot-}$ and $\text{Ru}(\text{bpy})_3^+$, respectively. Then $\text{Ru}(\text{bpy})_3^+$ is oxidized by $\text{SO}_4^{\cdot-}$ to generate the excited state $\text{Ru}(\text{bpy})_3^{2+*}$ of ECL emission. At the same time, $\text{SO}_4^{\cdot-}$ can also directly oxidize $\text{Ru}(\text{bpy})_3^{2+}$ into $\text{Ru}(\text{bpy})_3^{3+}$, which will then be annihilated with $\text{Ru}(\text{bpy})_3^+$ to produce $\text{Ru}(\text{bpy})_3^{2+*}$, leading to the final generation of ECL.⁴⁴

4.2. Luminol-Based System

Luminol is a commonly used and rather stable chemiluminescence reagent in various applications of biological engineering, chemical tracing, and criminal detection. Since scientists observed light emission when luminol was oxidized in 1928, this reagent had experienced a rapid growth in chemiluminescence-related investigations.⁴⁵ Subsequently, Kuwana discovered that the bright blue luminescence could also be generated when it was electrochemically oxidized in the presence of oxygen, which was the first report for luminol-based ECL phenomenon.⁴⁶

The most typical luminol-based ECL system is the luminol/ H_2O_2 system that has two possible mechanisms. In one mechanism, H_2O_2 can be electrochemically oxidized and then trigger ECL reaction, acting as both co-reactants (involved in electrode reactions) and oxidants to oxidize subsequent reagents. In another mechanism, H_2O_2 directly reacts with the electrochemical oxidative production of luminol to generate ECL, only acting as oxidants. The first one is

shown in Figure 3a. Luminol initially deprotonates in alkaline solution and is electrochemically oxidized at the anode to form a radical intermediate. At the same time, H_2O_2 is electrochemically oxidized into superoxide anion radical ($\text{O}_2^{\cdot-}$) which can then react with the above radical intermediates to generate excited 3-aminophthalate and finally emit blue fluorescence (425 nm).⁴⁷ In this process, H_2O_2 worked as a co-reactant. Meanwhile, the deprotonated H_2O_2 is able to directly react with the downstream products of luminol after two-step electron loss processes on the electrode to generate the excited 3-aminophthalate (as shown in Figure 3a). When H_2O_2 only acts as an oxidant, the intermediates that produce the excited 3-aminophthalate by removing N_2 are different. As shown in Figure 3b, it can be described that the intermediate diazoquinone is formed through electrochemical oxidation of luminol, which can react with H_2O_2 to produce luminol endoperoxide. After O–O bond cleavage, the excited species 3-aminophthalate is generated and then emits light. The presence of H_2O_2 could enable luminol to generate significant ECL emission whether or not it participates in the electrochemical reaction.⁴⁸ Therefore, this ECL system is commonly utilized in analyzing the concentration and activity of some enzymes which can produce H_2O_2 .

Recently, researchers have found that luminol can also produce ECL emission in the absence of H_2O_2 or other oxidizing reagents. In brief, the excited 3-aminophthalate will be created after successive electrochemical oxidation along with deprotonation of luminol and its reaction intermediates, still leading to light emission.⁵¹ Based on this mechanism, the detection of luminol in solutions by direct electrochemical oxidation may become a novel analytical method.

However, because light emission of the luminol-based ECL system can only be triggered in an alkaline solution, its applications have been severely restricted. In recent years, a representative luminol analogue, L012, was found to exhibit obvious ECL emission in an aqueous system. Additionally, it has the advantages of available moderate pH conditions (i.e., in neutral solution) and excellent biocompatibility, thus it is applied to detect H_2O_2 under physiological conditions and gradually replaces luminol in ECL-related (bio)research.⁵²

4.3. Nanomaterial-Based System

Compared with small molecule luminophores, nanomaterial-based ECL systems have gained considerable attention because of the tunable size and properties. Generally, three types of nanomaterials are discussed most, including quantum dots

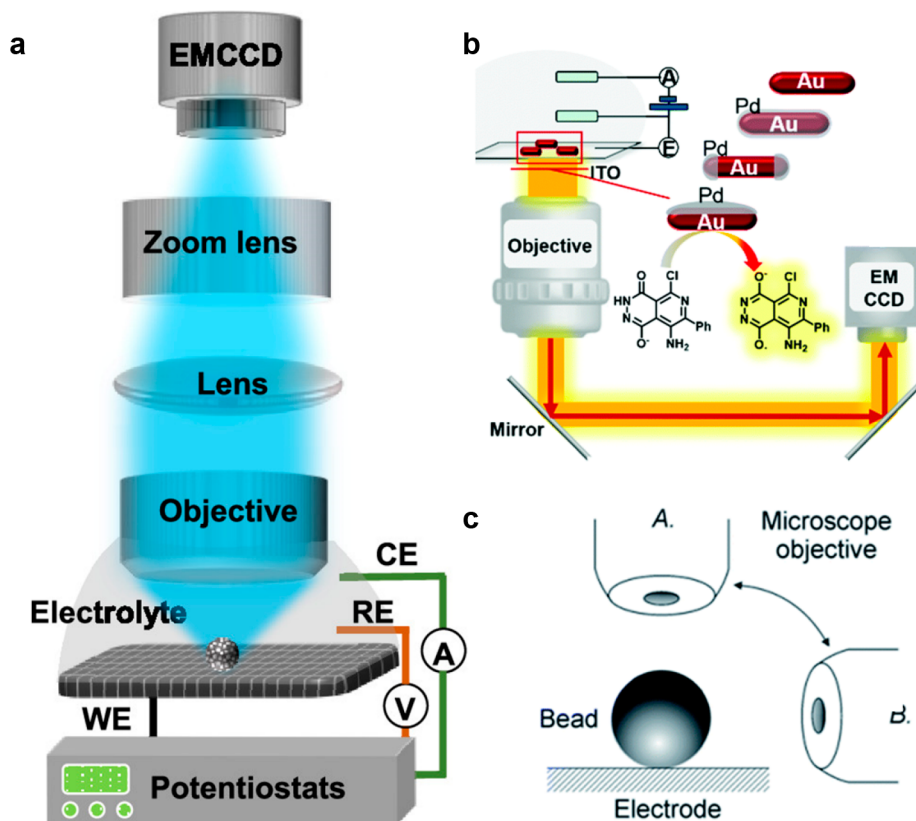


Figure 4. (a) Schematic image of the typical upright ECLM. Reprinted from ref 68. Copyright 2020 American Chemical Society. (b) Schematic image of the typical inverted ECLM. Reprinted with permission from ref 69. Copyright 2020 Royal Society of Chemistry. (c) Schematic image of the side-view ECLM. Reprinted with permission from ref 70. Copyright 2014 Royal Society of Chemistry.

(QDs), noble metal nanoclusters (NCs), and polymer dots (Pdots).

Semiconductor QDs are currently applied in various fields, such as photoelectrochemistry, bioimaging, and display devices due to their outstanding optical properties. In 2002, researchers first discovered that semiconductor Si QDs can emit ECL through both annihilation and co-reactant pathways.⁵³ Then a growing number of semiconductor QDs such as CdTe⁵⁴ and CdSe QDs⁵⁵ were found to have ECL emission properties. Benefitting from the quantum size effect, the emission wavelength of these QDs could be tuned from UV to NIR and thus could work as multicolor ECL probes. However, because these QDs always contain heavy metal that is not conducive for biological systems, scientists have adapted a series of non-metallic QDs such as graphene QDs (GQDs)⁵⁶ and carbon nitride QDs (C₃N₄ QDs)⁵⁷ with good ECL emission properties and biocompatibility for ECL-based biosensing, broadening the application range of quantum dot-based ECL systems.

Noble metal nanoclusters (Au,⁵⁸ Ag,⁵⁹ and Cu⁶⁰ NCs) reveal unique electrochemical and optical properties, especially long lifetime fluorescence and large Stokes shifts, making them gradually applied in the detection of small molecules, DNA, as well as proteins. These nanoclusters possess precise structure composition and controllable surface ligands, which help researchers understand the relation between ECL efficiency and nanocluster structures.

In recent years, Pdots have been quickly developed in areas such as cell labeling and drug delivery due to their features of excellent biocompatibility and easy modification. Besides, they

also exhibit good performance in ECL areas based on their tunable optical and electrochemical properties by the changing monomer size as well as the surface property. Nevertheless, their application has been seriously limited due to some severe disadvantages such as lower ECL efficiency and higher ECL initial potential. Therefore, researchers tried to optimize these materials by adapting some strategies like introducing donor–acceptor (D–A),⁶¹ aggregation-induced emission (AIE)-active,⁶² or resonance energy transfer-active moieties.⁶³ With much effort, Pdot-based ECL systems can be applied in the fields of biosensing and bioimaging successfully.

Dye-doped nanoparticles are also kinds of nanomaterial-based ECL emitters. The ECL emissions originate from the luminescence of doped dye molecules. Due to the nanoconfinement effect of the material, dye molecules can be enriched significantly, leading to a higher ECL efficiency. Meanwhile, the other performance of ECL can also be improved by altering the chemical and physical behaviors of the molecules.⁶⁴ Currently, many different dye-doped nanomaterials were developed as efficient ECL nanoemitters, and the most common one is Ru(bpy)₃²⁺-doped silica nanoparticle (RuDSN), which can be easily prepared based on the electrostatic interaction between Ru(bpy)₃²⁺ and silica, and has been widely applied in ECL analysis and sensing.⁶⁵

5. SETUP OF ECL MICROSCOPY

Combining the superiority of electrochemical and optical methods, ECL is widely used in the fields of biological and chemical analysis and therefore has high commercial values. However, only the information in bulk systems can be

obtained with traditional ECL analysis techniques. In recent years, with the development of optical microscopy imaging, researchers considered ECL as a kind of luminous form without an external light source and thus utilized it to establish a novel optical microscopy technique with near-zero background and high spatiotemporal resolution, extending ECL techniques to single objects at the micro/nanometer level.

The setup of ECLM mainly consists of two parts: an electrochemical system and an imaging system.⁶⁶ The electrochemical system contains an electrochemical workstation and traditional three-electrode system (a working electrode, an auxiliary electrode, and a reference electrode) to trigger ECL reactions. For the imaging system, three parts are essential, including the objective, the camera, and other optical elements making up the light path. First, according to the location of the objective, it can be divided into inverted ECLM, upright ECLM, and side-view ECLM (as seen in Figure 4). All of them have their own merits, for example, inverted ECLM can allow the use of any kind of electrolyte because the objective will not contact the electrolyte directly, while upright ECLM can adopt various kinds of electrodes. The side-view ECLM combining the labeling beads helped to elucidate the vertical distribution of ECL emission, further clarifying the mechanism of ECL reactions. Also, the camera is an important element in the imaging system. In the ECLM system, one of the most commonly used cameras is the CCD camera due to its low noise and excellent imaging quality. Another improvement is the EMCCD camera, which connects a string of gain registers behind the transfer register of CCD to amplify the signal and further improves the signal-to-noise (S/N), leading to a higher imaging sensitivity. The current EMCCD camera can even be utilized in the field of single-molecule fluorescence imaging; therefore, it is one of the best choices for ECLM imaging.⁶⁷ A complementary metal oxide semiconductor (CMOS) camera overcomes the problem of the high-cost CCD cameras. Also, compared with a CCD camera, a CMOS camera can reach a higher frame rate. As the technology continuously improves, the noise of the CMOS camera gradually decreases. A scientific CMOS (sCMOS) camera which appeared in 2009 is not inferior to the EMCCD camera in terms of signal detection ability with very weak photon level, showing the potential to replace the CCD camera in ECLM in the future.

Moreover, for the purpose of precise synchronous electrochemical sweeping and camera recording, a transistor–transistor logic (TTL) signal is desired,⁶⁶ which is generated from an electrochemistry workstation and then transferred to the external trigger channel of the camera. Another method to correlate the electrochemical signal and camera photos is to use a waveform generator and a data acquisition card to synchronously record two kinds of signals. In this way, frame-by-frame ECL photos under different voltages are obtained, similar to the ECL potential curves recorded by PMT.

Other optical elements such as lenses and mirrors are set according to an actual designed light path, which affects the magnification, spatial resolution, and signal collected efficiency. ECLM is a surface-confined technology due to the short lifetime of ECL-related reactive intermediates, thus the focal distance is in the vicinity of the electrode compared to other optical microscopies such as fluorescence microscopy. By adjusting the objective and lens groups, ECL signals can be obtained in different focal planes; however, the clearest ECL signal should be obtained on the electrode surface, and if the

ECL information extending away from the electrode surface is needed, some solutions such as using a catalytic route ECLM or raising the electrode surface temperature can be chosen, which will be discussed later. It is worth noting that all of the above-mentioned components need to be placed in a dark box to avoid interference from external light.⁵

6. DIVERSE APPLICATIONS OF ECL MICROSCOPY

The unprecedented prosperity of ECL techniques in diverse domains relies on simple equipment, high selectivity, and excellent signal-to-noise ratio due to the optoelectronic signal separation.^{4,71–73} However, the traditional modalities limited to the bulk ECL measurement of samples always ignore the ubiquitous heterogeneity in the single-object behavior. Thus, ECL imaging techniques with high spatiotemporal resolution combining ECL measurement and optical microscopy attract burgeoning interest from researchers. Whether it is an upright, an inverted, or a lateral-view microscope, the simple change in optical path and camera position are critical to achieve multidirectional and multiangle ECL imaging applications, the benefits of which will be described below. In the early 21st century, researchers mostly focused on the high throughput of ECLM to achieve sensing applications with a lower detection limit.^{74,75} Then, with the advancement of devices and commercial ECL labels, researchers utilized ECLM to provide a more profound understanding of ECL reaction mechanisms and single-particle imaging.^{70,76–78} Later in 2017, Sojic's group⁷⁹ promoted the field in the single-cell imaging by labeling ECL luminophores on the cell surface for the first time. Two decades of development have allowed ECL imaging to shine in sensing, mechanism elucidation, and analysis of single entities and cells, as well as the emergence of many other new ECLM crossover strategies, further demonstrating the great potential of this technique.

6.1. ECLM-Based Sensing Applications

At the early stage of ECLM, researchers mainly worked on using ECL as an optical readout recorded by a CCD or CMOS camera to visualize the sensing progress. The basic sensing principle embedded in these imaging measurements is that the ECL intensity is usually proportional to the sensing targets. The combination not only makes the sensing mechanism more authentic but also provides a lower detection limit at a micrometer scale, excellent spatial resolution, and high-throughput parallel analysis. Here, we will briefly introduce the sensing applications of ECL imaging techniques divided into three main methods: microelectrode arrays (MEAs), particle-based modification, and bipolar electrochemistry (BPE).

6.1.1. Microelectrode Arrays. In 2003, Szunerits et al.⁸⁰ constructed an array of electrode tips through chemical etching of an optical fiber bundle covered by gold. Employing Ru(bpy)₃²⁺ as luminophores and TPA as co-reactants, the ECL behavior at each apex of nanotips could be recorded by a CCD camera. Through adjusting the collection time of the CCD camera, the spatially resolved images could be obtained because of overcoming the diffusion overlap between single tips, providing the possibility to isolate the optical information from individual tips with the population of 6000. Later, a similar sensor array sputter-coated with ITO film was presented by Sojic's group, which could detect the concentration of hydrogen peroxide (H₂O₂) at the limit of 10 μM due to the linear relationship between the luminol ECL

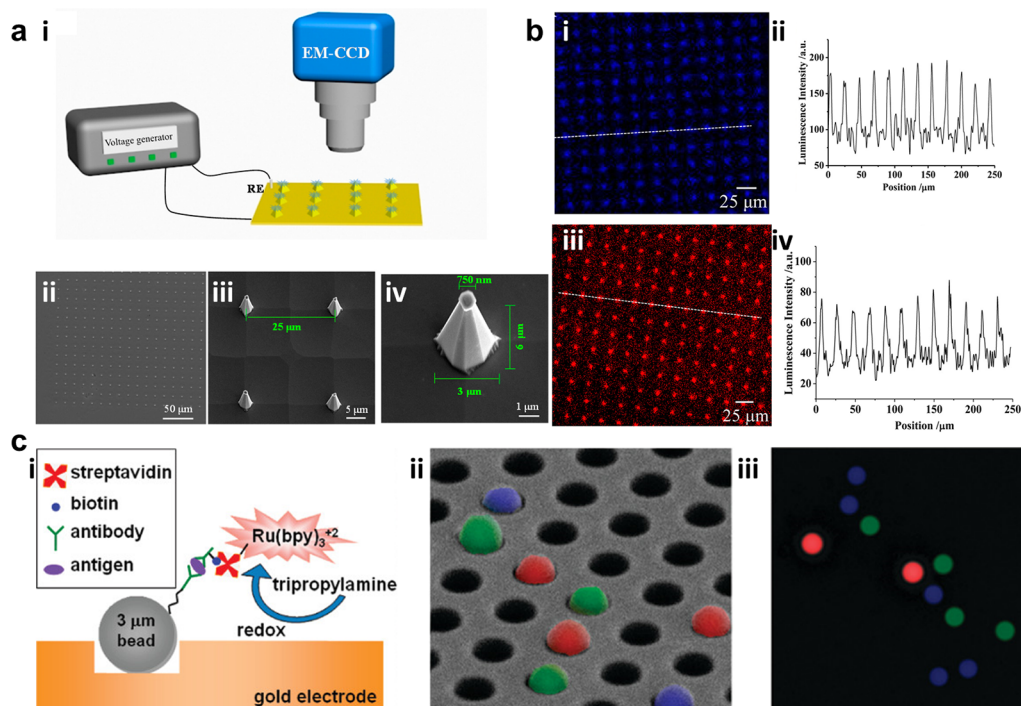


Figure 5. (a) (i) Device of nanoneedle electrodes for tip-enhanced ECL. (ii) Bright-field, (iii) scanning electron microscopy images for nanoneedles, and (iv) scanning electron microscopy image of an individual nanoneedle. (b) Corresponding local tip ECL images (i,iii) and the luminescence intensity analyzed along the white lines in ECL images (ii,iv), where (i,ii) is for 10 mM PBS containing 200 μM L012 and 2 mM hydrogen peroxide and (iii,iv) is for 10 mM PBS containing 10 mM $\text{Ru}(\text{bpy})_3^{2+}$ and 200 mM TPA. Reprinted from ref 82. Copyright 2017 American Chemical Society. (c) Strategy of sandwich immunoassay modification. (i) Schematic illustration and (ii) fluorescence images of different modified targets overlaid by false color, where blue is for anti-IL-8, red is for VEGF, and green is for TIMP-1. (iii) Corresponding ECL image for IL-8 in (ii). Reprinted from ref 85. Copyright 2009 American Chemical Society.

intensity and the H_2O_2 content.⁷⁴ Taking this work as the cornerstone, Chovin et al.⁷⁵ developed a gold nanoring surrounding array to achieve the remote detection of NADH which acted as strong synergistic co-reactants for $\text{Ru}(\text{bpy})_3^{2+}$. The generated ECL emission at the distal face located 6000 nanoapertures with gold rings transmitted through the fiber bundle by total internal reflection and was finally recorded by the camera in the proximal face, containing sub-micrometer spatial information.

Inspired by these works with an excellent linear relationship, low detection limits, and good reproducibility, researchers further explored more complicated electrode arrays. For example, Sentic et al.⁸¹ employed an e-beam lithographic procedure to construct a series of electrode arrays at the nanoscale on a boron-doped diamond (BDD) substrate. Benefiting from the improvement of mass transfer efficiency at the micro/nanoscale, they found that when TPA was used as a co-reactant, its concentration was inversely proportional to the thickness of the ECL light-emitting layer and thus a clearer pattern could be obtained.

Given the excellent performance of electrode arrays, a series of biosensors based on these substrate were fabricated by biomolecule modification. Zhang et al.⁸² modified glucose oxidase, lactate oxidase, and choline oxidase on a nanoneedle electrode array. The enzymes catalyzed the corresponding detection substances to generate H_2O_2 , which linearly enhanced the luminol ECL. Finally, the very high density sensing function of glucose, lactate, and choline could be achieved (Figure 5a,b). Ju's group designed a series of MEA based on the emission of Pdots.^{83,84} Luminol-doped polymer dots (L-Pdot) and diethylamine-coupled Pdots (N-Pdot) can

generate ECL emission with distinct wavelengths at different voltages. After the modified probes quenched the ECL emission of these Pdots, the targeted miRNA (miRNA-21 and miRNA-205) was added to recover the quenching ECL, enabling potential- and color-resolved quantitative detection of miRNA.⁸⁴ Also, using the quenching effect between dopamine (DA) and Pdots, they achieved confined MEA sensing of DA secreted from single cells.⁸³

6.1.2. Particle-Based Modification. Deiss et al.⁸⁵ developed a kind of sandwich immunoassay based on polystyrene (PS) beads. Briefly, the beads were first covered with the capturing antibodies for target antigens. After binding with corresponding antigens, additive biotinylated antibodies were added to link the streptavidin-modified $\text{Ru}(\text{bpy})_3^{2+}$ (SA-Ru) complex, which could generate ECL emission only when the analytes were present. Due to the capability of imaging single beads simultaneously on an optical fiber bundle coated with gold, multiplex detection of antigens was successfully achieved (Figure 5c). To obtain potentially and spectrally distinguished ECL signals, different luminophores could be mixed together. Guo et al.⁸⁶ mixed $\text{Ir}(\text{ppy})_3$ ($\text{ppy} = 2$ -phenylpyridine) with either $\text{Ru}(\text{bpy})_2(\text{dvbpy})_2^+$ or $\text{Ir}(\text{dFCF}_3\text{ppy})_2(\text{dtbbpy})^+$ to create the ECL emission with different potential and wavelengths. Combining the luminophore-loaded PS balls with a homogeneous sandwich immunoreaction, three antigens (carcinoembryonic antigen, α -fetoprotein, and β -human chorionic gonadotropin) could be detected simultaneously. This work opened a great possibility to fulfill multiple target imaging with the combination of potential-resolved and wavelength-resolved functions. Another novel work focused on visualizing a uranium rapid monitoring

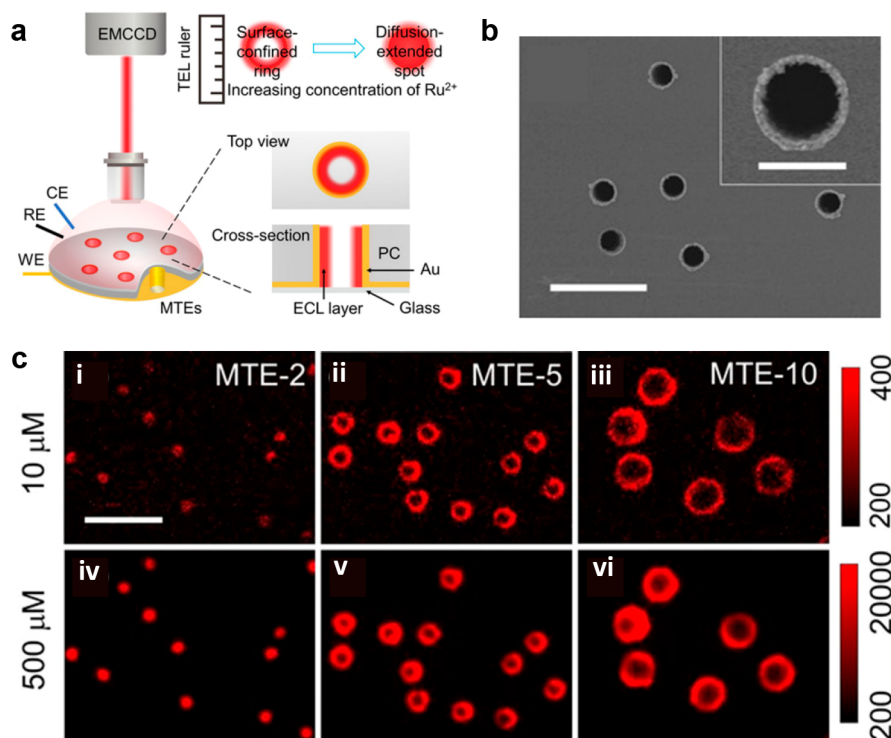


Figure 6. (a) Schematic image of measuring ECL layer through microtube electrodes. (b) Top view of microtubes with 5.4 μm diameter pores (termed as MTE-5). Scale bar (white): 20 μm . The inset image shows the magnified scanning electron microscopy image of single MTE-5 with a scale bar of 5 μm . (c) ECL images of MTE-2, MTE-5, and MTE-10 in 0.01 M phosphate buffer containing $\text{Ru}(\text{bpy})_3^{2+}$ (i–iii, 10 μM ; iv,v, 500 μM) and 25 mM TPA. Scale bar: 20 μm . MTE-2 and MTE-10 denote the microtubes with 2.3 and 10.6 μm diameter pores, respectively. Reprinted with permission from ref 25. Copyright 2021 Wiley-VCH.

system by modifying amidoxime on the polymer particles. Amidoxime could be functioned as a strong co-reactant as well as a capture group for the uranyl ion. Through the resonance energy transfer (RET) between UO_2^{2+} and ECL emission from the conjugated polymer backbone, the ultralow detection limit of 0.5 ng/L UO_2^{2+} could be achieved. This imaging method can act as a rapid warning system for radioactive elements in real water samples and thus has a great significance for early warning of public water safety.⁸⁷ These sensing works have strong practical applications, but their imaging tools are currently restricted to the macroscopic domains. Efforts are still needed for the intention to use microscopy imaging for guidance.

The sensing methods based on modifying the particles provide a selective strategy to get rid of the complex microarray electrodes but are limited by the low luminescence of the single objects. Therefore, many researchers dedicated to find ways to improve the ECL intensity on individual particles. Zanut et al.⁸⁸ synthesized two kinds of biotinylated $[\text{Ru}(\text{bpy})_3]^{2+}$ -doped silica nanoparticles by a reverse microemulsion method to exclude the interference of positive charges on a surface. When mimicking the commercial ECL-based immunoassay system, these nanoparticles showed 8.5 times ECL enhancement. Rebecani et al.⁸⁹ introduced functionalized carbon nanotubes (f-CNT) into the bead-based immunoassays. Because of the conductive layer around the beads created by the f-CNT, the $\text{Ru}(\text{bpy})_3^{2+}$ labeling complex could be oxidized directly, leading to the 4 times enhancement of the ECL signal. Similarly, Han et al.⁹⁰ demonstrated a new enhancement modality by decorating micrometric beads with $\text{Ru}(\text{bpy})_3^{2+}$ -grafted microgels. Com-

pared with traditional immuno-sandwich or amide bond-modifying beads, these microgel-functionalized beads showed a 9 times enhancement in ECL emission, which was attributed to the higher amount of ruthenium sites around the beads and the direct oxidation of $\text{Ru}(\text{bpy})_3^{2+}$ complex. The enhanced ECL imaging of single PS beads lays the foundation for the subsequent works focusing on the single entity studies by ECLM.

6.1.3. Bipolar Electrochemistry. BPE relies on placing a conductive object in the electric field to polarize both ends of this subject, thus inducing the simultaneous reduction and oxidation events.⁹¹ Some outstanding advantages of BPE include the avoidance of the direct contact with electrodes and asymmetric electroactivity. Under the action of BPE, a glassy carbon bead can be driven by hydrogen bubbles generated at one extremity to promote mechanical motion and emit ECL luminescence at the other extremity due to the reaction between $\text{Ru}(\text{bpy})_3^{2+}$ luminophores and enzymatically produced NADH. In this way, an interesting ECL “swimmer” was established to detect the concentration gradient of glucose spatially.^{92,93}

Because of no limitation to the number of electrodes, BPE is often used in combination with arrays to obtain a better sensitivity and detection capability. The initial work proposed by Chow et al.⁹⁴ utilized the hybridization of cDNA labeled with electrocatalytic Pt nanoparticles which could reduce oxygen at the cathode and thus trigger the ECL reaction in the anode to achieve the observation of DNA presence. Since then, a lot of works integrating BPE and arrays have been reported to detect H_2O_2 ,⁹⁵ including several quinones,⁹⁶ prostate specific antigen (PSA),⁹⁷ etc.

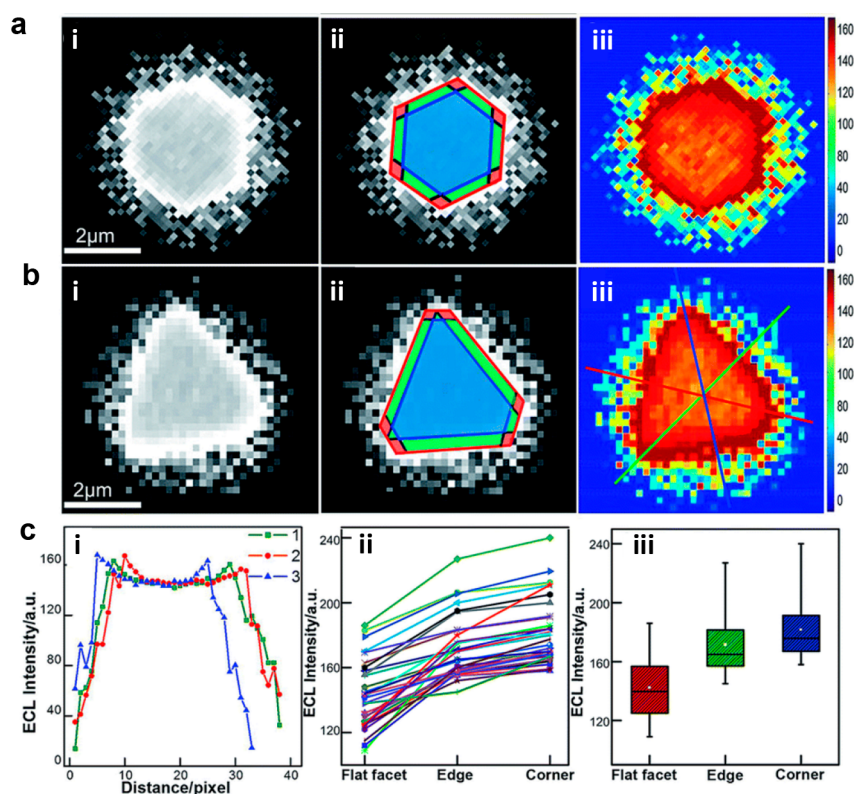


Figure 7. (a) (i) ECL image of a single hexagonal nanoplate. Scale bar: $2\ \mu\text{m}$. (ii) Different regions of ECL image (i) marked by red for corners, green for edges, and blue for flat surface facet. (iii) ECL intensity of 2D spatial distribution from Matlab. (b) (i) ECL image of a single triangular nanoplate. Scale bar: $2\ \mu\text{m}$. (ii) Different regions of ECL image (i) marked by red for corners, green for edges, and blue for flat surface facet. (iii) ECL intensity of 2D spatial distribution from Matlab. (c) (i) Corresponding ECL intensity along the lines marked in (b) (iii). (ii) Statistical data of ECL intensity for different regions in 35 nanoplates. (iii) Box charts of ECL intensity for different regions. Reprinted with permission from ref 102. Copyright 2019 Royal Society of Chemistry.

6.2. ECLM-Based Exploration for the Mechanism

After developing the prototype for labeling the luminophores on single beads, researchers were inspired by the visualization ability of ECLM, thus deploying this technique to gain deeper insight into the ECL reaction. Sentic et al.⁷⁰ reconstructed a 3D cartography of $\text{Ru}(\text{bpy})_3^{2+}$ -labeled PS microspheres with an orthogonal side-view configuration. Through the intuitive observation of the uneven distribution of ECL on the beads and the simulation calculation, compared with the DBAE system, the significance of TPA and its cation radicals for the regulation of the light-emitting layer is clarified. This work showed that only luminophores located at $\sim 3\ \mu\text{m}$ along the z axis contribute to the signal, implying the importance of the TPA^{+} lifetime, and further motivated them to modify the ECL layer by simply changing the concentration of buffer capacity.⁷⁷ In the basic mechanism of ECL when immobilizing the luminophores, the essential role of the TPA deprotonation process has already been recognized. Thus, the ECL intensity increased with the lower ECL concentration of phosphate buffer (PB). However, the ECL intensity still decreased as the electrochemical reaction proceeded, due to the passivation to the system. Dutta et al.⁹⁸ subsequently applied an easy cathode pulse method to regenerate the electrode surface and recover the ECL intensity. Due to using the same 3D imaging device, the whole process could be clearly verified by “seeing”. Zanut et al.⁷⁸ discovered an additional highly efficient pathway of the ECL classic co-reactant system (i.e., TPA as co-reactant) appearing extremely close to the electrode ($< 1\ \mu\text{m}$). Taking

advantage of the tip generation–surface emission technique along with aided quantum computation proof, they determined a rather short-living dipropylamine radical contributing to the 8 times enhancement in ECL. Guided by this result, they selected the particular branched amine DPIBA as co-reactant and increased the ECL emission by 128%.

In addition to exploring the reaction mechanism by labeling beads and changing the position of the objective, another innovative method is to directly observe the thickness of the emission layer through microtube electrodes (Figure 6a).²⁵ These vertical electrodes can avoid troublesome optical path variations, allowing to simply view the pattern changing from a ring to a spot upon increasing the concentration ratio of $\text{Ru}(\text{bpy})_3^{2+}$ to co-reactants through an upright microscope (Figure 6c). The thickness of the ECL layer using the TPA co-reactant changed from 3.1 to $>4.5\ \mu\text{m}$, while for the system of the DBAE co-reactant, which had a shorter lifetime, was nearly unchanged, similar to the result measured by beads. Later, microtube electrodes were developed into ultra-high-density microporous electrode arrays, which could also perform the same mechanism analysis, showing great potential in sensing and diagnostic domains.⁷⁶

6.3. ECLM-Based Application for Single Entities

In 2008, Bard et al.¹⁹ first observed the collision behavior of Pt nanoparticles on ITO electrodes through the ECL method. Each photon spike was found to correlate with the collision process. In the same year, Chang et al.⁹⁹ first used ECLM to observe the ECL emission of single polymer nanoparticles,

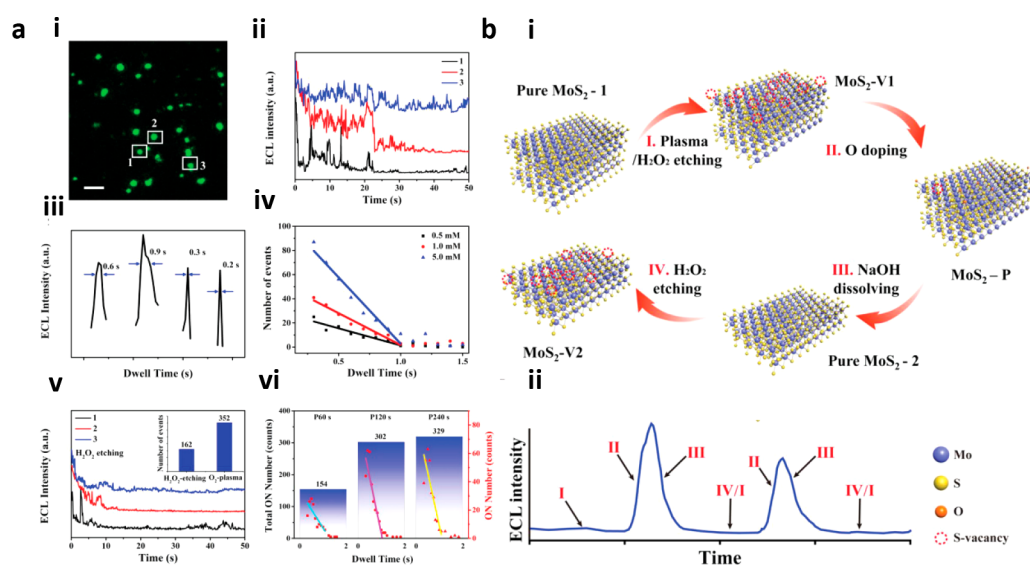


Figure 8. (a) Analysis of ECL bursts controlled by sulfur vacancy and oxygen doping. (i) ECL image of MoS_2 after oxygen plasma treatment ($\text{MoS}_2\text{-P}$) in 10 mM PBS containing $200\ \mu\text{M}$ L012 and 5 mM H_2O_2 . Scale bar: $10\ \mu\text{m}$. (ii) Successive change of ECL intensity of three selected particles. (iii) Corresponding dwell time of random ECL bursts. (iv) Corresponding ON events with dwell time in different H_2O_2 concentrations. (v) ECL intensity change after H_2O_2 etching for 18 h. The inset shows the different ON events number between H_2O_2 etching and O_2 plasma treatment for 10 particles. (vi) Total ON events (black) and separate ON events (red) for 10 particles with different O_2 plasma treatment time: 60, 120, and 240 s. The correlation between ON events and dwell time could also be found. (b) Schematic illustration of ECL bursts, where (i) indicates the mechanic pathway and (ii) indicates the corresponding ECL intensity change. Reprinted with permission from ref 106. Copyright 2021 Wiley-VCH.

F8BT in the acetonitrile system containing TPRA as co-reactants. Although the former work mentioned above may lack the spatial information and the latter work was limited in the organic system, they opened the door of ECLM to observe the single entities. At the early stage of imaging single entities by ECLM, the implementation overlapped with the sensing application or deciphering mechanism through single bead modification. However, these reports mainly focused on the micrometer scale of imaging. With the continuous improvement of technology, there emerged a growing need for smaller-sized emitters and applications that were no longer limited to sensing. Among these, research on gold particles came out first because of their good catalytic performance and easy control of size. In 2015, Wilson et al.¹⁰⁰ first achieved the ECL imaging of electrocatalysis ability on single gold nanowires. ECLM has a unique property with no need for an extrinsic illumination source, integrating high-throughput optical imaging with electrochemistry, making up for the deficiencies of scanning electrochemical microscopy. Moreover, gold particles could catalyze the ECL reaction to be distinguished from the background signal. Therefore, ECLM is an outstanding observation tool for gold nanowires. By removing the surfactant layer of purchased gold nanowires and coating with a polymer blend to protect nanowires from surface oxidation, a relatively stable ECL emission of a single gold nanowire could be successfully obtained. After that, Pan et al.¹⁰¹ synthesized a series of gold particles of different sizes from 30 to 300 nm and employed the digital simulation to determine the effect of particle size and electrode potential. Individual gold nanoparticles exhibited ECL heterogeneity, once again demonstrating the superiority of ECL imaging. This heterogeneity was also manifested in 2D gold nanomaterials. Due to the auxiliary numerical simulation excluding the influence of uneven voltage distribution on the surface of the microelectrodes, the observed nonuniform ECL distribution

on 2D gold nanoplates could be attributed to the difference in the catalytic activity site on the surface of single objects (Figure 7).¹⁰² However, these monometal materials were often unable to maintain stable light emission for a long time. Thus, Zhu et al.¹⁰³ used ECLM to observe a bimetallic material called the Janus particle. Because the different electron transfer rate of Pt and Au could lead to the fluid slip around the asymmetric metal interfaces, the Janus particles were sheltered from passivation and exhibited higher ECL intensity and were more stable than single Pt and Au particles. Similar results can also be obtained from bimetallic Pd–Au nanorods (NRs).⁶⁹ Compared with Pd-tipped Au NRs and Pd-covered Au NRs, anisotropic Pd–Au Janus NRs showed the best ECL catalytic performance because of their unique nanostructure.

In addition to metal particles, the high spatiotemporal resolution of ECLM allowed the evaluation of the catalytic properties of materials ranging from two-dimensional materials^{104–106} to lower-dimensional quantum dots (QDs).^{107,108} The underlying principle for these reports was similar, taking advantage of the heterogeneous active sites on materials to catalyze water or H_2O_2 , followed by generating intermediates that could act as co-reactants for luminol or its analogous L-012 to emit ECL. Based on this basic paradigm, Chen et al.¹⁰⁷ first compared the catalytic performance of different QDs (i.e., CdSe, CdTe, CdTeSe). The CdTeSe QDs had a more suitable valence band position and more defects on the surface which alter the surface energy and reduce the formation energy of intermediates. Accordingly, the CdTeSe QDs exhibited the strongest ECL intensity. Later, they synthesized a ZnO crystal of different facets to show the correlation between electrocatalytic performance and the exposed facets. The experimental and theoretical results verified that the ZnO (002) facets were superior to the ZnO (100) facets in terms of catalytic rate.¹⁰⁸ Zhu et al.¹⁰⁵ controlled the generation of redox-induced defects on the surface of reduced graphene

oxide (rGO) nanosheets by changing the voltage applied. Using the perturbation ECL imaging method, the fluctuation of charge transfer resistance on individual rGO microsheets with more redox-induced defects was revealed, i.e., more defects contributing to a higher charge transfer resistance. Inspired by this work, they subsequently introduced oxygen plasma irradiation to modulate the surface defects on rGO. Moreover, heterogeneous active sites adsorbing different amounts of luminophores and co-reactants would produce distinguished intensities of luminescence. By controlling the exposure time to 0.2 s, the separated ECL emission region could be successfully obtained to overcome the diffusion effect, resulting in a high spatial resolution of 400 nm.¹⁰⁴ Recently, they focused on the ECL behavior of transition metal dichalcogenides (TMDCs).¹⁰⁶ In the case of molybdenum disulfide (MoS_2), oxidation can occur easily because the strength of the oxidation bond was higher than that of the sulfide bond. Coincidentally, oxygen-doped sites could produce strong ECL luminescence while sulfur sites cannot, making ECLM an excellent imaging tool to study kinetic processes for the oxidation process. The authors observed the ECL bursts generated on the surface of MoS_2 , together with theoretical calculations, revealed that the oxygen doping process was an intermittent process of millisecond scale and also clarified for the first time the joint effect between the edge and the basal plane on the oxidation process (Figure 8).

Despite the good catalytic ability of these entities aforementioned enabling single-particle ECL imaging, the luminophores of the ECL system are still insufficient, mainly limited to $\text{Ru}(\text{bpy})_3^{2+}$ and luminol. Therefore, there are also works devoted to extending the application of ECL using other nanoemitters. Among them, Ma et al.⁶⁸ synthesized C_3N_4 as the cathode luminophore, first observing the ECL blinking phenomenon during electrocatalytic hydrogen evolution reactions. The appearance of this ECL on/off phenomenon obeys a power-law function distribution and correlates to the generation, growth, and collapse of hydrogen nanobubbles generated on C_3N_4 hollow nanospheres. Because of the correlation between ECL blinking and hydrogen generation rate, the authors loaded other catalysts such as AuPd, NiS, and Pt on C_3N_4 and later successfully evaluated their catalytic performance.

In addition to the exploration of the catalytic properties of materials, the merits of ECLM can promote many novel applications. One of them is to detect transient electrochemical events. Conventionally, ultra-microelectrode techniques cannot realize the high spatial and temporal resolution simultaneously. In other words, ultra-microelectrode analysis can provide spatial information but at the expense of temporal resolution and vice versa. Ma et al.²⁰ instead observed the collision process of $\text{Ru}(\text{bpy})_3^{2+}$ -doped silica nanoparticles (RuDSNs) by ECLM. Unlike the electrode background that may result from metal particle catalyzing ECL reactions, these RuDSNs could achieve zero background ECL detection of collision events. The authors investigated the variability in the ECL emission of RuDSNs with different particle sizes and $\text{Ru}(\text{bpy})_3^{2+}$ doping amounts by a homemade ECLM combined with a scanning electron microscopy colocalization strategy. The fast time-resolving capability of the ECLM allowed the single-particle collisions to be divided into spike and staircase types, corresponding to elastic and viscous collisions, respectively. This visualization technique exemplified its great potential in electrochemical analysis. Another interesting work

used ECLM to observe the crystalline molecular wires made of cyclometalated iridium(III) complexes. These wires could act as both ECL emitters and active waveguides, which allowed the long-range ECL to propagate inside the molecule over 100 μm , showing great potential in electrochemical analysis without contact.¹⁰⁹

6.4. ECLM-Based Application for Single Cells

As the ECLM technology on imaging single particles continues to mature, extending it to the cellular domain has become a major impetus for researchers. Although fluorescence microscopy is the most well-developed method for single-cell imaging, the dependence on external light sources makes it difficult to eliminate the background of the cell itself. At this point, the advantages of ECLM that has a near-zero optical background and simple equipment are proven. Currently, ECLM reports in the field of single-cell imaging can be classified into negative image mode and positive image mode. Here, we will also follow this classification to briefly introduce this technology at the single-cell level plus new trends to image the intracellular structure by ECLM.

6.4.1. Positive Image Mode with Labeling Process.

The positive imaging mode tends to show a brighter ECL distribution of the target cells to distinguish them from the background electrodes. Gaining the experience for labeling PS balls by immuno-sandwich modality, Valenti et al.⁷⁹ first applied this labeling process to cells in 2017. Compared to the FLM, the ECLM did not show the entire cell surfaces but the cell borders in the vicinity to the electrodes due to the limited lifetime of TPA co-reactants (the ECL mechanism obeyed the LOP pathway as discussed before) and the intrinsic cellular blockage of co-reactant diffusion. Later, they added a surfactant, Triton-X, to improve the permeability of cell membranes so that the co-reactants could transport through the cell membrane to create ECL images of whole basal membranes. Because the ECLM had a special feature of surface confinement, it provided more details of cell basal membrane in contrast to FLM.¹⁸ This approach paved the new way for ECLM to develop single-cell analysis, but its luminescence intensity and stability were still in need of improvement. For this reason, Wang et al.¹¹⁰ synthesized tertiary amine conjugated polymer dots (TEA-Pdots) that inserted the co-reactants (i.e., TEA) into the backbone of emitters (i.e., Pdots) to shorten the distance between these two reactants. Through a dual intramolecular electron transfer process, the TEA-Pdots exhibited unprecedented high ECL intensity compared to that of the classic ECL system of equivalent concentration, thus extending the application to evaluate the specific protein on a cell membrane. Han et al.¹¹⁰ discussed the pivotal role of the adsorbed electrogenerated species on the electrode surface after prolonged electrolysis. After imposing the cathodic pulse to remove these species, the ECL intensity would be recovered soon.

When such a labeling paradigm was developed taking advantage of the specific binding of antigens and antibodies or biotin and streptavidin, the idea of detecting targeted proteins or antibodies at the single-cell level became clarified. Liu et al.¹¹¹ designed g- C_3N_4 and Au@L012 as two ECL emitters functionalized by recognition units to specifically recognize epidermal growth factor receptor (EGFR) and phosphatidylserine (PS), respectively. When apoptosis occurred, the PS on the cell membrane would be everted. Due to the separation of ECL emission between g- C_3N_4 and Au@L012, the potential-

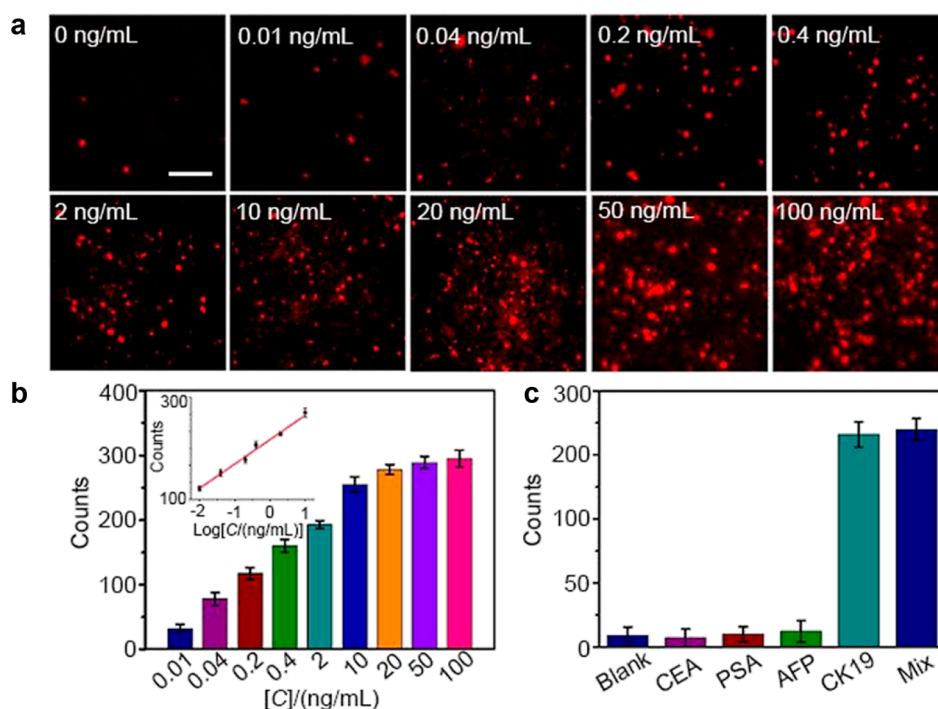


Figure 9. (a) Single-molecule ECL images of different concentrations of CK 19. The luminophores are RuDSN/AuNPs. The electrodes used are ITO. Scale bar: 5 μm . (b) ECL counts of CK 19 from 0.01 to 100 ng/mL. The inset diagram indicates the linear relationship between ECL counts and the logarithm of CK 19 concentrations (0.01 to 10 ng/mL). (c) Specificity tests with target CK 19 (0.4 ng/mL) and other proteins (40 ng/mL). Reprinted from ref 112. Copyright 2021 American Chemical Society.

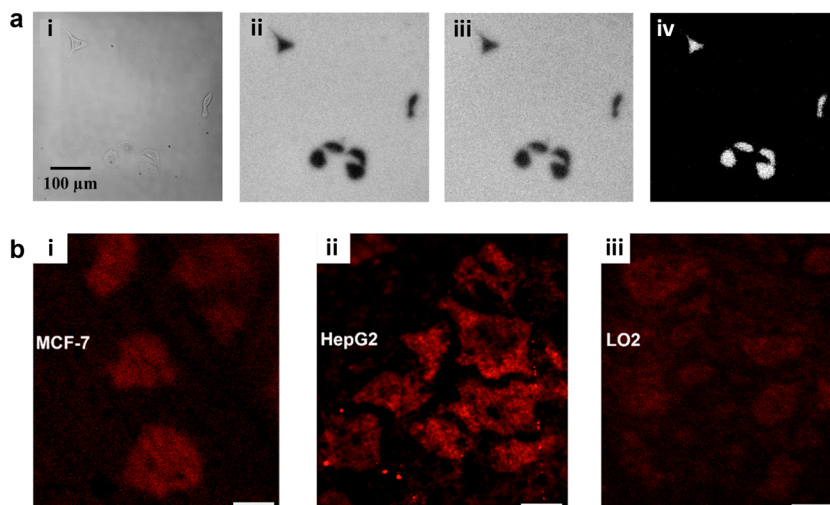


Figure 10. (a) Images of HeLa cells on ITO. (i) Bright-field (BF) image of HeLa cells. (ii) ECL image of the same HeLa cells in (i) with 200 μM L012. (iii) ECL image of the same HeLa cells in (i) with 200 μM L012 after stimulating cells by PMA. (iv) ECL image by subtracting (ii) from (iii). Scale bar: 100 μm . Reprinted from ref 117. Copyright 2015 American Chemical Society. (b) ECL images of MCF-7 (i), HepG2 (ii), and LO2 (iii) cultured on the closed BPE system after stimulation by PMA (1 $\mu\text{g}/\text{mL}$). The ECL system includes 1 mM Ru(bpy)₃²⁺ and 20 mM DBAE in 0.1 M PB (pH 7.0). Exposure time: 1 s, scale bars: 30 μm . Reprinted from ref 120. Copyright 2022 American Chemical Society.

resolved ECL images of the cell apoptosis process could be achieved. Liu et al.¹¹² enriched Ru(bpy)₃²⁺ into the RuDSNs, which were decorated with Au nanoparticles to enhance the conductivity and identify the targets (Figure 9). This nanocomposite amplified the ECL emission so that even single biomolecules on the cell membrane were visualized. In addition, Ru(bpy)₃²⁺@SiO₂/Au nanoparticles were also designed for sensing the prostate-specific antigens in combination with BPE at the single-cell level.¹¹³ Recently, Li et al.¹¹⁴ utilized the nanoconfinement effect of metal–organic frame-

works (MOFs) to obtain the Ru(bpy)₃²⁺-embedded MOF complex (RuMOFs) with extreme bright ECL emission. With the aid of RuMOFs targeted to single proteins of living cells, even the dynamic imaging of single molecular movements could be successfully achieved.

To extend the application of the ECLM with a limited imaging range near the electrode surface, another type of ECLM labeling method using the catalytic pathway was developed. As mentioned above, in catalytic pathway, the ECL layer will be mainly decided by the long life-span Ru(bpy)₃³⁺,

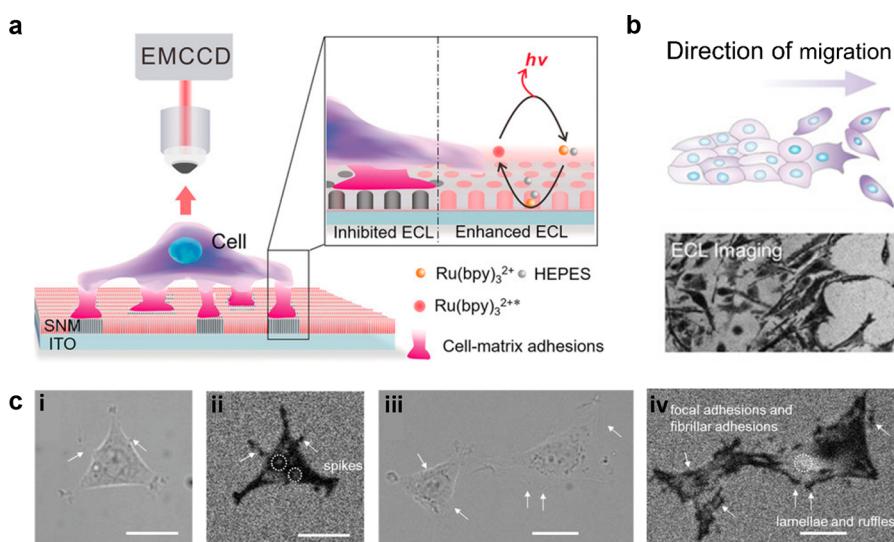


Figure 11. (a) Typical schematic diagram of negative image mode in ECL system. The cell here was cultured on the SNM/ITO in Ru(bpy)₃²⁺ and HEPES solution. (b) Schematic illustration and corresponding ECL image of cell adhesion showing the direction of collective migration. (c) Corresponding bright-field images (i,iii) and ECL images (ii,iv) of cell adhesion in 10 mM PBS (pH 7.4) containing 50 μM Ru(bpy)₃²⁺ and 20 mM HEPES. Scale bar: 20 μm. More detailed structure such as spikes and focal adhesions could only be seen in ECL images. Reprinted with permission from ref 21. Copyright 2020 Wiley-VCH.

leading to a thicker luminescent region. Ma et al.¹¹⁵ prepared nitrogen-doped carbon dots (NCDs) modified by the PSBP peptide as the co-reactants to recognize PS externalization. Through the catalytic route, the upper membrane of cells could also be imaged by their homemade ECLM setup. Likewise, Chen et al.¹¹⁶ synthesized biocompatible co-reactants composed of Au nanoflowers loaded by guanine-rich ssDNA. The DNA employed here could act as not only the co-reactants because of its abundant guanine contents but also the aptamer to target the carcinoembryonic antigen (CEA). After incubation with different types of cells, these artificial DNA co-reactants not only specifically differentiated the healthy and tumor cells but also maintained the ability to image the cell membrane far away from the electrode surface.

6.4.2. Positive Image Mode without Labeling Process. ECL emission is generated by electrochemical reactions, thus offering the possibility to get rid of relatively tedious labeling processes. One of the keys is to find substances that are relevant to the cellular physiological process and can act as co-reactants or luminophores. H₂O₂ is a suitable target which is correlated with many biological processes, such as enzyme catalytic reactions, cell lysis and apoptosis, local efflux events from living cells, etc., and can also be the co-reactants of luminol or L012. After stimulated by phorbol myristate acetate (PMA), HeLa cells could produce extra H₂O₂, resulting in the H₂O₂ efflux. When luminol met with H₂O₂ in the space between the cells and the electrodes, the ECL emission was enhanced, leading to the mapping pictures of H₂O₂ efflux at the single-cell level by removing the background signal. Using this method, parallel analysis of the activated membrane cholesterol could also be achieved by adding cholesterol oxidase to the solution because H₂O₂ would also be generated by the reaction between membrane cholesterol and the oxidase (as shown in Figure 10a).¹¹⁷ However, the resolution of ECL imaging was still limited owing to the molecular diffusion effect, and then the same group tried to use vertically ordered silica pore arrays to limit the range of ECL generation, which improved the resolution to the submicron level.¹¹⁸

The positive image in the works mentioned above relied on the image difference before and after H₂O₂ release to subtract cell background due to the spatial blockage of the cells. However, this image processing operation may reduce the image accuracy because living cells constantly change in their morphologies and adhesions. The image difference is only validated if spatial blockage of the cells remained unchanged with time elapsing. To address this issue, Liu et al.¹¹⁹ developed a direct imaging strategy by modifying the chitosan film on the electrodes. The chitosan film enlarged the distance between the cell basal membrane and the electrode, thus allowing more luminophores to accumulate below the cell. After stimulating cells on the FTO electrode by *N*-formylmethionyl leucyl phenylalanine (fMLP), the direct positive images of targets were obtained immediately. Another strategy to in situ image cells in the positive mode is to resort to a bipolar nanoelectrode array.¹²⁰ In a closed bipolar array divided by gold nanoelectrodes, the authors platinized gold electrodes in the cathode section and incubated the cells there. The oxygen generated through electrocatalysis was temporarily aggregated under the cells because of their steric hindrance and thus was related to a higher ECL intensity at the anode and achieved the positive images of the cell contours.¹²⁰ Similarly, through stimulating living cells to generate H₂O₂ efflux, the ECL images of different cell types (i.e., HeLa, HepG2, MCF-7, and L02 cells) correlated with the amount of H₂O₂ released, as shown in Figure 10b.¹²⁰

Although the cells could remain somewhat viable during these efforts, the problems posed by electrical damage at high voltages and a less stable ECL system were fatal. Thus, single particles were used to ameliorate these problems. For example, Cui et al.¹²¹ first synthesized semiconductor titanium dioxide particles, which was difficult to passivate by electricity, to achieve stable ECL luminescence. Then these particles provided stable sensing signals for local efflux when applied to the cells. Zhang et al.¹²² utilized single lithium iron phosphate (LiFePO₄, LFP) nanoparticles to realize the ECL positive image of efflux at a relative low potential of 0.5 V,

owing to the promotion of the ECL reaction caused by lithium migration.

Except for local efflux events, this imaging principle could be used to show other processes. Gao et al.¹²³ encapsulated PMA and doxorubicin (DOX) in mesoporous silica. When the carrier was specifically recognized by nucleophiles inside the cell, PMA and DOX could then be released, followed by the production of excess reactive oxygen species to induce apoptosis and react with luminol, thus enabling ECL imaging of the drug release process. Another source of H₂O₂ could be the reduction reagent of oxygen by imposing the negative potential. Based on sequential potential steps, Hiramoto et al.¹²⁴ realized the ECL imaging of cell respiratory activity, demonstrating that the black areas appearing near the cell spheroids were the result of oxygen consumption by cellular respiration.

6.4.3. Negative Image Mode. A special image mode of ECLM is the negative image mode, which has the simplest imaging process. In the negative image mode, the cell could be seen as a steric hindrance to block the ECL reaction, so the cell outline appears as a black image under the ECLM compared to the bare area of electrodes (Figure 11a). Because the reaction layer of ECL always depends on the limited lifetime of intermediates, it is more surface-confined to the electrode than bright-field (BF) image and is therefore well suited to study the dynamics of cell adhesion. In order to eliminate the effect of electric stimulation and cytotoxicity from the ECL reaction system, as shown in Figure 11, Ding et al.²¹ cultured PC12 cells on the silica nanochannel membrane (SNM)-modified ITO electrodes (SNM/ITO) and used HEPES as co-reactants. With the prerequisites that the cells remained viable, the authors studied the variation of cell–matrix adhesion associated with some physiology processes due to the natural advantage for imaging the cell adhesion by ECLM at the subcellular level. By adding trypsin, the spatial difference in cell–matrix adhesion during digestion process were dynamically demonstrated. Also, by a typical wound healing assay, the direction change in cell–matrix adhesion during collective migration was further identified by ECLM, showing that even cells far from the scratch front tended to move forward. ECLM here provided the feasibility to analyze the cell physiological process and determine the specific molecular functions through the transmutation of cell adhesion morphology. Thus, they later changed the terminal groups tethered on SNM/ITO to explore the specific recognition of integrins to different surfaces. Through the morphology change of cell adhesion, it was found that $\alpha 6$, $\alpha 5$, and $\alpha 1$ subunits sensed SNM, RGD/OEG, and APTES electrode surfaces, respectively.¹²⁵ Gao et al.¹²⁶ then observed the process of cell shrinking, crumpling, and detaching from the electrode surface by adding H₂O₂, along with the cell aggregation by electrical stimulation. Chen et al.¹²⁷ subsequently proposed a novel method employing ECL to drive photodynamic therapy, where ECL can be used both as an optical readout and as an internal light source for the photosensitizer chlorin e6 (Ce6) by effective energy transfer process. Similarly, the therapeutic efficacy of the Ce6 was assessed by the clear identification of deformation, expansion, detachment, and membrane blebbing of PC12 and MCF-7 cells due to the capability of ECLM to monitor cell adhesions.

Certainly this simple unlabeled strategy could be used to image other physiological process or cellular components, such as the tube formation of vascular endothelial cells on hydrogel

scaffold¹²⁸ and subcellular organelles.²² Compared to the imaging results of fluorescent dye, the negative imaging mode, named the shadow ECLM method by Ma et al.,²² could detect smaller mitochondria. However, these studies all benefited from the fact that the ECLM imaging range is limited to the vicinity of the electrode surface, making it difficult to observe cell structures far from the electrode. To address this problem, Ding et al.⁴⁰ modulated the ECL layer by regulating the ratio of luminophores and co-reactants. When the concentration of luminophores increased to some extent, the catalytic pathway appeared and thus extended the ECL layer away from the electrode surface. In this context, the spatially resolved imaging of cell–matrix and cell–cell junctions could be easily achieved. Additionally, Ma et al.¹²⁹ regulated the thickness of ECL layer (TEL) through the heated electrodes. The electrode temperature (T_e) would increase from 20 to 60 °C. The increasing T_e not only extended the TEL because of the faster diffusion rates but also accelerated the electrochemical kinetics, leading to clearer cell contours. Thus, by simply tuning T_e , the cell topography at different heights could be achieved due to the fine and reversible response of TEL to temperature under different reaction paths.

6.4.4. New Trends for Intracellular Imaging. The application of ECLM inside cells is hampered by the fact that the reaction species must be electrically excited while being hindered by the cell membrane. Scientists have been trying to develop a strategy for ECLM that can achieve intracellular imaging. A little earlier, in order to measure the intracellular glucose contents, Xu et al.¹³⁰ and Xia et al.¹³¹ introduced cell-sized microelectrode arrays to ECLM system, making internal glucose of individual cells flow into each microwells by breaking the cells to obtain the corresponding ECL images. Obviously, this method did not meet the expectation of *in situ* imaging the interior of cells. And the electrical damage was another serious problem blocking ECLM to image the intracellular change of living cells. Using bipolar nanoelectrode arrays, incubating the cells at one section can maintain the cellular activity to some extent, as described previously.¹²⁰ However, in fact, conventional BPE needs strict size limitations for conductive objects,¹³² and thus a higher voltage may be required for micro- and nanoscale objects, which can still cause damage when directly used in biological systems. Fortunately, wireless nanopore electrodes offer the hope.^{133–135} Thanks to the confinement effect of nanopipettes, the polarization at the tip is locally enhanced, thus reducing the applied potential and narrowed down the range of electrical damage significantly. Even 90% of the voltage drop of the nanoelectrode designed by Ying et al.¹³⁵ would occur at the tip, and using this asymmetric BPE amplification strategy, they achieved the monitoring of electron transfer process in living cells. He et al.¹³⁶ first developed an ultra-microelectrode with a tip of 1–2 μm , containing luminophores inside and sputter-coated with Au to enhance conductivity. The tip could then break through the cell membrane barrier and met with the internal H₂O₂. Due to the contact with gold and the application of positive voltage, the ECL images could be recorded, showing the possibility to visualize the intracellular H₂O₂ in situ. Later, they developed more sophisticated platinum-deposited nanopipette tips in combination with bipolar ECL to realize the wireless detection of intracellular components, i.e., H₂O₂, glucose, and the activity of sphingomyelinase.¹³⁷ The porous structure of the tip not only effectively reduced the voltage required for bipolar electrochemistry but also generated electro-osmotic flow to

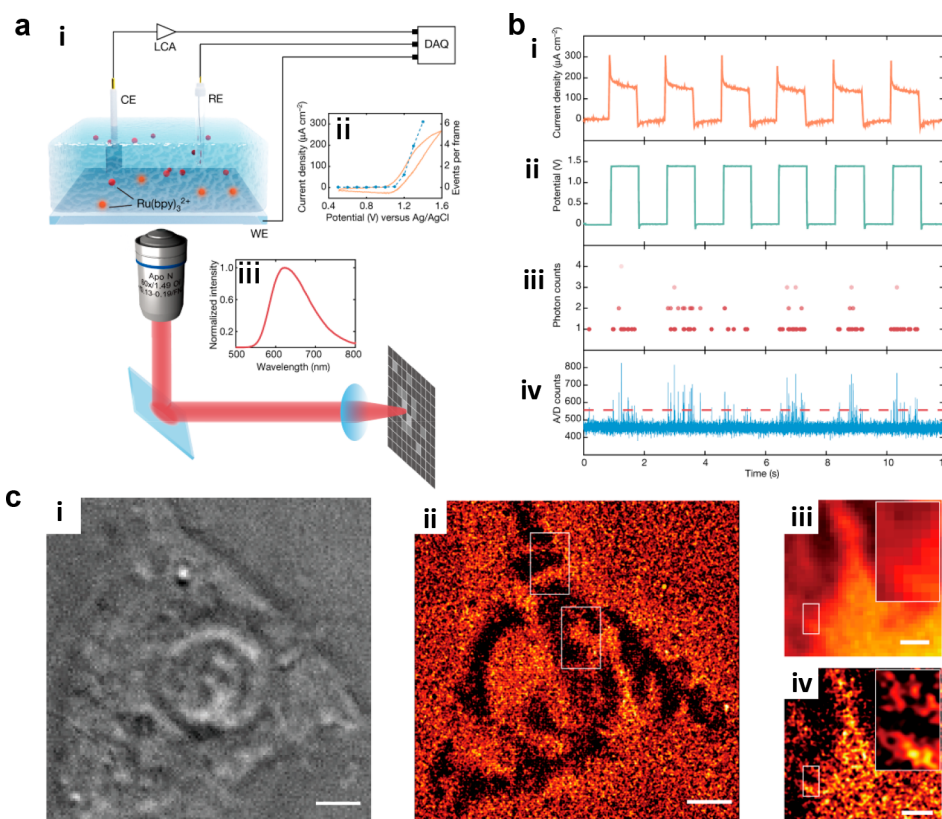


Figure 12. (a) (i) Schematic image of the single-molecular ECL setup. (ii) Cyclic voltammetry (CV) measurement and corresponding ECL signal in 50 μM $\text{Ru}(\text{bpy})_3^{2+}$ with 50 mM TPA with exposure time of 0.507 ms. (iii) ECL emission spectrum of $\text{Ru}(\text{bpy})_3^{2+}$. (b) (i) Current density, (ii) applied voltage, (iii) photon counts, and (iv) analog-to-digital (A/D) counts at the same time. (c) Corresponding (i) bright-field image and (ii) super-resolution ECL image for the same HEK293 cell on an ITO surface. Scale bar (white): 5 μm . (iii) Diffraction-limited ECL image and (iv) super-resolution ECL image of the same region. Scale bar (white): 2 μm . Reprinted with permission from ref 24. Copyright 2021 Springer Nature.

promote the inflow of cytosol. However, in situ imaging of the internal cell structure is still challenging by these devices. Ma et al.¹¹⁵ invented a bio-co-reactant-enhanced ECLM which efficiently exploited the difference in the intrinsic content of amino-rich biomolecules of intracellular structures. Through a catalytic pathway, the $\text{Ru}(\text{bpy})_3^{2+}$ luminophores could electro-oxidize at the electrode surface to create the stable enough $\text{Ru}(\text{bpy})_3^{3+}$, which could transport to the inside of cells and react with amino-rich DNA as co-reactants. As time elapsed, substructures richer in co-reactants such as the nucleus would show stronger ECL emission, displaying the hierarchical ECL spatial distribution. This tool could also be used to observe the dynamic electroporation process since the co-reactants were separated by the cell membrane, promoting the novel use of ECLM in single-cell analysis.

6.5. Other ECLM-Based Strategies

The development of a technology is inseparable from the reference of other technologies. For ECLM, inspired by the existing techniques of electrochemical microscopy, thin film interferometer, FLM, etc., it has developed many other new crossover strategies with excellent performance.

Generally, to obtain a positive ECL image of specific antigens distributed on cell membrane, the labeling methods would be processed. However, Zhang et al.¹³⁸ creatively integrated ECLM with electrochemical capacity method, utilizing the potential drop across the double layer (V_{dl}) to image the CEA antigens on cell membrane with the detection limit lower to 1 pg. The binding area caused a drop in specific

capacity and resulted in a higher V_{dl} , corresponding to a higher ECL intensity. In this way, the nonlabeling ECL images of CEA distribution could be achieved easily.

In addition to drawing on electrochemical-related techniques, ECL can also be combined with interference spectroscopy to reach the vertical nanoscale resolution.¹³⁹ ECL emission from luminophores and that from the electrode surface reflection could induce self-interference phenomenon, which was then analyzed by matrix propagation model to derive the thickness of ECL layer. With the increase of $\text{Ru}(\text{bpy})_3^{2+}$ concentration, the ECL layer varied from ~ 350 nm to nearly 1 μm , which was inaccessible using conventional ECL measurements.

For $\text{Ru}(\text{bpy})_3^{2+}$, its ECL emission is at the same excited state as fluorescence, so some development of ECLM originates from the reference of fluorescence microscopy. Han et al.¹⁴⁰ discovered the ECL loss during the photobleaching, showing the linear correlation of these two phenomenon, which also implied the possibility for developing ECLM with photobleaching methods. Later, Dong et al.²⁴ achieved super-resolution ECLM according to single-molecule fluorescence localization technique (Figure 12). When applying to the cell imaging, the motion of cell adhesion with the temporal resolution of 12 s and spatial resolution of 150 nm was recorded. This work first breaking the diffraction limit in ECLM paved the way for super-resolved ECLM, which removed the tedious labeling process and the intervention of an excitation light source compared to the super-resolution FLM. Later, the same technique was processed on the single

gold plates¹⁴¹ to gain the structure–activity relationship of catalysts. With the high spatial resolution, the heterogeneity of the surface reactivities could be obtained. Moreover, the dynamic catalytic hotspot changes when adding potassium chloride to etch Au oxides could be recorded through time-lapse, which may be helpful for designing the catalysts. Another kind of super-resolution ECLM was based on super-resolution radial fluctuation (SRRF).¹⁴⁰ By processing the SRRF method, the spatial resolution achieved 100 nm so that the different catalytic ability at the subparticle level could be easily visualized. After analyzing the reconstructed ECL images, the variation at different parts of the gold plates was attributed to the characteristics of high-index facets and growth-dependent underlying surface defects. Meanwhile, the high temporal resolution helped to dissect the relationship between catalytic sites and stability. Most higher activity sites, however, showed the lower stability, showing the opposite trend between catalytic activity and stability.

7. CONCLUSIONS AND OUTLOOK

Due to the unique merits of ECL measurements and microscopy devices, ECLM is equipped with high throughput, high spatiotemporal resolution, and high sensitivity. Through the understanding of basic mechanisms in the ECLM field, device setup and diverse applications discussed in this review, it is no doubt that the ECLM is growing fast. Until now, ECLM has realized super-resolution imaging and single-molecule imaging with the assistance of advanced devices and sophisticated algorithms, showing the stunning potential of this technique.

Nevertheless, there is still a long way to go for ECLM. One problem is how to overcome the diffusion effect of dissolved ECL species, which could be the key to improve the spatial resolution. In some early papers containing microelectrode arrays of ECL, the researchers reduced the collection time to obtain the spatial isolated ECL spots, implying a solution to this problem. The coupling of ultrahigh speed camera may be a good choice, but there is another problem becoming the stumbling block that ECL is always a weak emission process. To solve this problem, new nanoemitters with high ECL intensity needs to be developed. Dual intramolecular electron transfer strategy is a good example, which shortened the distance between reactants and finally magnified ECL intensity. Along with advanced detection devices such as EMCCD or sCMOS, the weak emission is expected to surmount in the future. Third, the more practical and complexed (bio)-applications should be achieved with tireless endeavor. Currently, the high sensitivity and fast response to the surface changes render ECLM an ideal method for detection of fingerprints, which is most likely to put into practical use.^{142,143}

However, the gap between experimental results and other practical applications still requires to be bridged. The biggest obstacle here is how to address the electrical damage and the ECL toxicity for biological systems. Thus, modalities like wireless ECL propagation, bipolar electrochemistry, etc., flourished in the past few years and will keep going in the coming days. Meanwhile, other biocompatible ECL systems with low applied potential along with the novel electrode materials are also worth waiting for. In addition, the biological exploration of ECLM nowadays mainly focus on the microscopic biological structures (i.e., cells and organelles). Upscaling metabolic processes from animals to humans and macroscopic structures including tissues and organs is brand

new territory for ECLM, which may accelerate the experimental findings to the clinical practice.

Indeed, the difficulties encountered when the technology is budding always carry abreast opportunities and challenges. We believe ECLM will continue to prosper in more creative realms at single entity level and bring us new approaches to solve more practical problems. We appreciate all the efforts in ECL field that could make the world a better place.

AUTHOR INFORMATION

Corresponding Authors

Cheng Ma – State Key Laboratory of Analytical Chemistry for Life Science, School of Chemistry and Chemical Engineering, Nanjing University, Nanjing 210023, P.R. China; School of Chemistry and Chemical Engineering, Yangzhou University, Yangzhou 225002, P.R. China; orcid.org/0000-0001-5729-8483; Email: chengma@nju.edu.cn

Jun-Jie Zhu – State Key Laboratory of Analytical Chemistry for Life Science, School of Chemistry and Chemical Engineering, Nanjing University, Nanjing 210023, P.R. China; orcid.org/0000-0002-8201-1285; Email: jjzhu@nju.edu.cn

Authors

Xiaodan Gou – State Key Laboratory of Analytical Chemistry for Life Science, School of Chemistry and Chemical Engineering, Nanjing University, Nanjing 210023, P.R. China

Zejing Xing – State Key Laboratory of Analytical Chemistry for Life Science, School of Chemistry and Chemical Engineering, Nanjing University, Nanjing 210023, P.R. China

Complete contact information is available at:
<https://pubs.acs.org/10.1021/cbmi.2c00007>

Author Contributions

Xiaodan Gou and Zejing Xing contributed equally to this work. The manuscript was written through contributions of all authors.

Notes

The authors declare no competing financial interest.

ACKNOWLEDGMENTS

This work was supported by the National Natural Science Foundation of China (Grant Nos. 21834004, 22174061, and 21904063), the Natural Science Foundation of Jiangsu Province (Grant No. BK20190279), Yangzhou University Interdisciplinary Research Foundation for Chemistry Discipline of Targeted Support (yzuxk202009), and Foundation of State Key Laboratory of Analytical Chemistry for Life Science (Grant No. SKLACLS2201).

VOCABULARY

Electrochemiluminescence (ECL): A light emission process initiated by electrochemical reactions

Co-reactant: Species that could generate the reductants or oxidants to help the luminophores emit light in the small potential window

Low-oxidation potential (LOP) route: A mechanism for Ru(bpy)₃²⁺ and TPrA system that only co-reactant TPrA involved in electrochemical reactions during ECL process

Electron-multiplying CCD (EMCCD): The camera setup that contains multiple gain registers behind the transfer register of CCD to amplify the signal and further improves the signal-to-noise (S/N)

TEL: The thickness of ECL layer usually decided by the distribution of the excited state of luminophores

REFERENCES

- (1) Schneckenburger, H.; Weber, P.; Wagner, M.; Schickinger, S.; Richter, V.; Bruns, T.; Strauss, W. S. L.; Wittig, R. Light exposure and cell viability in fluorescence microscopy. *J. Microsc.* **2012**, *245* (3), 311–318.
- (2) Song, L. L.; Hennink, E. J.; Young, I. T.; Tanke, H. J. PHOTBLEACHING KINETICS OF FLUORESCHEIN IN QUANTITATIVE FLUORESCENCE MICROSCOPY. *Biophys. J.* **1995**, *68* (6), 2588–2600.
- (3) Richter, M. M. Electrochemiluminescence (ECL). *Chem. Rev.* **2004**, *104* (6), 3003–3036.
- (4) Liu, Z.; Qi, W.; Xu, G. Recent advances in electrochemiluminescence. *Chem. Soc. Rev.* **2015**, *44* (10), 3117–42.
- (5) Ma, C.; Cao, Y.; Gou, X.; Zhu, J. J. Recent Progress in Electrochemiluminescence Sensing and Imaging. *Anal. Chem.* **2020**, *92* (1), 431–454.
- (6) Wang, H.; Pu, G.; Devaramani, S.; Wang, Y.; Yang, Z.; Li, L.; Ma, X.; Lu, X. Bimodal Electrochemiluminescence of G-CNQDs in the Presence of Double Coreactants for Ascorbic Acid Detection. *Anal. Chem.* **2018**, *90* (7), 4871–4877.
- (7) Ma, C.; Wu, W.; Peng, Y.; Wang, M. X.; Chen, G.; Chen, Z.; Zhu, J. J. A Spectral Shift-Based Electrochemiluminescence Sensor for Hydrogen Sulfide. *Anal. Chem.* **2018**, *90* (2), 1334–1339.
- (8) Liu, Y.; Wang, M.; Nie, Y.; Zhang, Q.; Ma, Q. Sulfur Regulated Boron Nitride Quantum Dots Electrochemiluminescence with Amplified Surface Plasmon Coupling Strategy for BRAF Gene Detection. *Anal. Chem.* **2019**, *91* (9), 6250–6258.
- (9) Liu, Y.; Chen, X.; Ma, Q. A novel amplified electrochemiluminescence biosensor based on Au NPs@PDA@CuInZnS QDs nanocomposites for ultrasensitive detection of p53 gene. *Biosens. Bioelectron.* **2018**, *117*, 240–245.
- (10) Peng, L.; Yuan, Y.; Fu, X.; Fu, A.; Zhang, P.; Chai, Y.; Gan, X.; Yuan, R. Reversible and Distance-Controllable DNA Scissor: A Regenerated Electrochemiluminescence Biosensing Platform for Ultrasensitive Detection of MicroRNA. *Anal. Chem.* **2019**, *91* (5), 3239–3245.
- (11) Song, X.; Li, X.; Wei, D.; Feng, R.; Yan, T.; Wang, Y.; Ren, X.; Du, B.; Ma, H.; Wei, Q. CuS as co-reaction accelerator in PTCA-K2S2O8 system for enhancing electrochemiluminescence behavior of PTCA and its application in detection of amyloid-beta protein. *Biosens. Bioelectron.* **2019**, *126*, 222–229.
- (12) Zhang, A.; Guo, W.; Ke, H.; Zhang, X.; Zhang, H.; Huang, C.; Yang, D.; Jia, N.; Cui, D. Sandwich-format ECL immunosensor based on Au star@BSA-Luminol nanocomposites for determination of human chorionic gonadotropin. *Biosens. Bioelectron.* **2018**, *101*, 219–226.
- (13) Wang, L.; Liu, D.; Sun, Y.; Su, J.; Jin, B.; Geng, L.; Song, Y. Y.; Huang, X.; Yang, M. Signal-On Electrochemiluminescence of Self-Ordered Molybdenum Oxynitride Nanotube Arrays for Label-Free Cytosensing. *Anal. Chem.* **2018**, *90* (18), 10858–10864.
- (14) Cui, C.; Chen, Y.; Jiang, D.; Zhu, J. J.; Chen, H. Y. Attomole Antigen Detection Using Self-Electrochemiluminous Graphene Oxide-Capped Au@L012 Nanocomposite. *Anal. Chem.* **2017**, *89* (4), 2418–2423.
- (15) Chen, S.; Chen, X.; Zhang, L.; Gao, J.; Ma, Q. Electrochemiluminescence Detection of Escherichia coli O157:H7 Based on a Novel Polydopamine Surface Imprinted Polymer Biosensor. *ACS Appl. Mater. Interfaces* **2017**, *9* (6), 5430–5436.
- (16) Liu, Y.; Wei, Y.; Cao, Y.; Zhu, D.; Ma, W.; Yu, Y.; Guo, M. Ultrasensitive electrochemiluminescence detection of Staphylococcus aureus via enzyme-free branched DNA signal amplification probe. *Biosens. Bioelectron.* **2018**, *117*, 830–837.
- (17) Zhang, Z.; Ma, C.; Xu, Q.; Zhu, J. J. Recent progress in electrochemiluminescence microscopy analysis of single cells. *Analyst* **2022**, *147* (13), 2884–2894.
- (18) Voci, S.; Goudeau, B.; Valenti, G.; Lesch, A.; Jovic, M.; Rapino, S.; Paolucci, F.; Arbault, S.; Sojic, N. Surface-Confined Electrochemiluminescence Microscopy of Cell Membranes. *J. Am. Chem. Soc.* **2018**, *140* (44), 14753–14760.
- (19) Fan, F.-R. F.; Bard, A. J. Observing Single Nanoparticle Collisions by Electrogenerated Chemiluminescence Amplification. *Nano Lett.* **2008**, *8* (6), 1746–1749.
- (20) Ma, C.; Wu, W.; Li, L.; Wu, S.; Zhang, J.; Chen, Z.; Zhu, J. J. Dynamically imaging collision electrochemistry of single electrochemiluminescence nano-emitters. *Chem. Sci.* **2018**, *9* (29), 6167–6175.
- (21) Ding, H.; Guo, W.; Su, B. Imaging Cell-Matrix Adhesions and Collective Migration of Living Cells by Electrochemiluminescence Microscopy. *Angew. Chem. Int. Ed. Engl.* **2020**, *59* (1), 449–456.
- (22) Ma, Y.; Colin, C.; Descamps, J.; Arbault, S.; Sojic, N. Shadow Electrochemiluminescence Microscopy of Single Mitochondria. *Angew. Chem. Int. Ed.* **2021**, *60* (34), 18742–18749.
- (23) Zhang, J.; Arbault, S.; Sojic, N.; Jiang, D. Electrochemiluminescence Imaging for Bioanalysis. *Annu. Rev. Anal. Chem. (Palo Alto Calif)* **2019**, *12* (1), 275–295.
- (24) Dong, J.; Lu, Y.; Xu, Y.; Chen, F.; Yang, J.; Chen, Y.; Feng, J. Direct imaging of single-molecule electrochemical reactions in solution. *Nature* **2021**, *596* (7871), 244–249.
- (25) Guo, W.; Zhou, P.; Sun, L.; Ding, H.; Su, B. Microtube Electrodes for Imaging the Electrochemiluminescence Layer and Deciphering the Reaction Mechanism. *Angew. Chem. Int. Ed. Engl.* **2021**, *60* (4), 2089–2093.
- (26) Harvey, N. Luminescence during Electrolysis. *J. Phys. Chem.* **1929**, *33* (10), 1456–1459.
- (27) Hercules, D. M. Chemiluminescence Resulting from Electrochemically Generated Species. *Science* **1964**, *145* (3634), 808–809.
- (28) Bouffier, L.; Sojic, N. Chapter 1. Introduction and Overview of Electrogenerated Chemiluminescence. *Analytical Electrogenerated Chemiluminescence* **2019**, 1–28.
- (29) Ritchie, E. L.; Pastore, P.; Wightman, R. M. Free Energy Control of Reaction Pathways in Electrogenerated Chemiluminescence. *J. Am. Chem. Soc.* **1997**, *119* (49), 11920–11925.
- (30) Beideman, F. E.; Hercules, D. M. Electrogenerated chemiluminescence from 9,10-diphenylanthracene cations reacting with radical anions. *J. Phys. Chem.* **1979**, *83* (17), 2203–2209.
- (31) Hoytink, G. J. Electrochemiluminescence of aromatic hydrocarbons. *Discuss. Faraday Soc.* **1968**, *45* (0), 14–22.
- (32) Chang, M.-M.; Saji, T.; Bard, A. J. Electrogenerated chemiluminescence. 30. Electrochemical oxidation of oxalate ion in the presence of luminiscers in acetonitrile solutions. *J. Am. Chem. Soc.* **1977**, *99* (16), 5399–5403.
- (33) Leland, J. K.; Powell, M. J. Electrogenerated Chemiluminescence: An Oxidative-Reduction Type ECL Reaction Sequence Using Tripropyl Amine. *J. Electrochem. Soc.* **1990**, *137* (10), 3127–3131.
- (34) Rubinstein, I.; Bard, A. J. Electrogenerated chemiluminescence. 37. Aqueous ecl systems based on tris(2,2'-bipyridine)ruthenium(2+) and oxalate or organic acids. *J. Am. Chem. Soc.* **1981**, *103* (3), 512–516.
- (35) Akins, D. L.; Birke, R. L. Energy transfer in reactions of electrogenerated aromatic anions and benzoyl peroxide. Chemiluminescence and its mechanism. *Chem. Phys. Lett.* **1974**, *29* (3), 428–435.
- (36) Lytle, F. E.; Hercules, D. M. CHEMILUMINESCENCE FROM THE REDUCTION OF AROMATIC AMINE CATIONS AND RUTHENIUM(III) CHELATES*,†. *Photochem. Photobiol.* **1971**, *13* (2), 123–133.
- (37) Prier, C. K.; Rankic, D. A.; MacMillan, D. W. Visible light photoredox catalysis with transition metal complexes: applications in organic synthesis. *Chem. Rev.* **2013**, *113* (7), 5322–63.

- (38) Tokel, N. E.; Bard, A. J. Electrogenerated chemiluminescence. IX. Electrochemistry and emission from systems containing tris(2,2'-bipyridine)ruthenium(II) dichloride. *J. Am. Chem. Soc.* **1972**, *94* (8), 2862–2863.
- (39) Noffsinger, J. B.; Danielson, N. D. Generation of chemiluminescence upon reaction of aliphatic amines with tris(2,2'-bipyridine)ruthenium(III). *Anal. Chem.* **1987**, *59* (6), 865–868.
- (40) Ding, H.; Zhou, P.; Fu, W.; Ding, L.; Guo, W.; Su, B. Spatially Selective Imaging of Cell-Matrix and Cell-Cell Junctions by Electrochemiluminescence. *Angew. Chem. Int. Ed. Engl.* **2021**, *60* (21), 11769–11773.
- (41) Miao, W.; Choi, J.-P.; Bard, A. J. Electrogenerated Chemiluminescence 69: The Tris(2,2'-bipyridine)ruthenium(II), (Ru(bpy)₃²⁺)/Tri-n-propylamine (TPrA) System Revisited A New Route Involving TPrA^{•+} Cation Radicals. *J. Am. Chem. Soc.* **2002**, *124* (48), 14478–14485.
- (42) Liu, X.; Shi, L.; Niu, W.; Li, H.; Xu, G. Environmentally friendly and highly sensitive ruthenium(II) tris(2,2'-bipyridyl) electrochemiluminescent system using 2-(dibutylamino)ethanol as co-reactant. *Angew. Chem. Int. Ed. Engl.* **2007**, *46* (3), 421–4.
- (43) Kebede, N.; Francis, P. S.; Barbante, G. J.; Hogan, C. F. Electrogenerated chemiluminescence of tris(2,2' bipyridine)-ruthenium(II) using common biological buffers as co-reactant, pH buffer and supporting electrolyte. *Analyst* **2015**, *140* (21), 7142–5.
- (44) White, H. S.; Bard, A. J. Electrogenerated chemiluminescence. 41. Electrogenerated chemiluminescence and chemiluminescence of the Ru(2,21 - bpy)₃²⁺-S₂O₈²⁻ system in acetonitrile-water solutions. *J. Am. Chem. Soc.* **1982**, *104* (25), 6891–6895.
- (45) Marquette, C. A.; Blum, L. J. Applications of the luminol chemiluminescent reaction in analytical chemistry. *Anal Bioanal Chem.* **2006**, *385* (3), 546–54.
- (46) Kuwana, T.; Epstein, B.; Seo, E. T. ELECTROCHEMICAL GENERATION OF SOLUTION LUMINESCENCE. *J. Phys. Chem.* **1963**, *67* (10), 2243–2244.
- (47) Cui, H.; Zou, G.-Z.; Lin, X.-Q. Electrochemiluminescence of Luminol in Alkaline Solution at a Paraffin-Impregnated Graphite Electrode. *Anal. Chem.* **2003**, *75* (2), 324–331.
- (48) Marquette, C. A.; Blum, L. J. Electro-chemiluminescent biosensing. *Anal Bioanal Chem.* **2008**, *390* (1), 155–68.
- (49) Ding, H.; Su, B.; Jiang, D. C. Recent Advances in Single Cell Analysis by Electrochemiluminescence. *Chemistryopen* **2022**, No. e202200113.
- (50) Ding, H.; Guo, W. L.; Su, B. Electrochemiluminescence Single-Cell Analysis: Intensity- and Imaging-Based Methods. *ChemPlusChem.* **2020**, *85* (4), 725–733.
- (51) Wróblewska, A.; Reshetnyak, O. V.; Koval'chuk, E. P.; Pasichnyuk, R. I.; Błażejowski, J. Origin and features of the electrochemiluminescence of luminol – Experimental and theoretical investigations. *J. Electroanal. Chem.* **2005**, *580* (1), 41–49.
- (52) Nishinaka, Y.; Aramaki, Y.; Yoshida, H.; Masuya, H.; Sugawara, T.; Ichimori, Y. A New Sensitive Chemiluminescence Probe, L-012, for Measuring the Production of Superoxide Anion by Cells. *Biochem. Biophys. Res. Commun.* **1993**, *193* (2), 554–559.
- (53) Ding, Z.; Quinn, B. M.; Haram, S. K.; Pell, L. E.; Korgel, B. A.; Bard, A. J. Electrochemistry and Electrogenerated Chemiluminescence from Silicon Nanocrystal Quantum Dots. *Science* **2002**, *296* (5571), 1293–1297.
- (54) Liu, X.; Jiang, H.; Lei, J.; Ju, H. Anodic Electrochemiluminescence of CdTe Quantum Dots and Its Energy Transfer for Detection of Catechol Derivatives. *Anal. Chem.* **2007**, *79* (21), 8055–8060.
- (55) Jie, G.; Li, L.; Chen, C.; Xuan, J.; Zhu, J. J. Enhanced electrochemiluminescence of CdSe quantum dots composited with CNTs and PDDA for sensitive immunoassay. *Biosens. Bioelectron.* **2009**, *24* (11), 3352–8.
- (56) Li, L.-L.; Ji, J.; Fei, R.; Wang, C.-Z.; Lu, Q.; Zhang, J.-R.; Jiang, L.-P.; Zhu, J.-J. A Facile Microwave Avenue to Electrochemiluminescent Two-Color Graphene Quantum Dots. *Adv. Funct. Mater.* **2012**, *22* (14), 2971–2979.
- (57) Xu, H.; Liang, S.; Zhu, X.; Wu, X.; Dong, Y.; Wu, H.; Zhang, W.; Chi, Y. Enhanced electrogenerated chemiluminescence behavior of C₃N₄ QDs@ C₃N₄ nanosheet and its signal-on aptasensing for platelet derived growth factor. *Biosens. Bioelectron.* **2017**, *92*, 695–701.
- (58) Wang, T.; Wang, D.; Padelford, J. W.; Jiang, J.; Wang, G. Near-Infrared Electrogenerated Chemiluminescence from Aqueous Soluble Lipoic Acid Au Nanoclusters. *J. Am. Chem. Soc.* **2016**, *138* (20), 6380–3.
- (59) Chen, A.; Ma, S.; Zhuo, Y.; Chai, Y.; Yuan, R. In Situ Electrochemical Generation of Electrochemiluminescent Silver Nanoclusters on Target-Cycling Synchronized Rolling Circle Amplification Platform for MicroRNA Detection. *Anal. Chem.* **2016**, *88* (6), 3203–10.
- (60) Zhao, M.; Chen, A. Y.; Huang, D.; Zhuo, Y.; Chai, Y. Q.; Yuan, R. Cu Nanoclusters: Novel Electrochemiluminescence Emitters for Bioanalysis. *Anal. Chem.* **2016**, *88* (23), 11527–11532.
- (61) Omer, K. M.; Ku, S. Y.; Cheng, J. Z.; Chou, S. H.; Wong, K. T.; Bard, A. J. Electrochemistry and electrogenerated chemiluminescence of a spirobifluorene-based donor (triphenylamine)-acceptor (2,1,3-benzothiadiazole) molecule and its organic nanoparticles. *J. Am. Chem. Soc.* **2011**, *133* (14), 5492–9.
- (62) Wang, Z.; Feng, Y.; Wang, N.; Cheng, Y.; Quan, Y.; Ju, H. Donor-Acceptor Conjugated Polymer Dots for Tunable Electrochemiluminescence Activated by Aggregation-Induced Emission-Active Moieties. *J. Phys. Chem. Lett.* **2018**, *9* (18), 5296–5302.
- (63) Wang, N.; Wang, Z.; Chen, L.; Chen, W.; Quan, Y.; Cheng, Y.; Ju, H. Dual resonance energy transfer in triple-component polymer dots to enhance electrochemiluminescence for highly sensitive bioanalysis. *Chem. Sci.* **2019**, *10* (28), 6815–6820.
- (64) Dong, B.; Mansour, N.; Huang, T. X.; Huang, W.; Fang, N. Single molecule fluorescence imaging of nanoconfinement in porous materials. *Chem. Soc. Rev.* **2021**, *50* (11), 6483–6506.
- (65) Zhang, L.; Dong, S. Electrogenerated Chemiluminescence Sensors Using Ru(bpy)₃²⁺ Doped in Silica Nanoparticles. *Anal. Chem.* **2006**, *78* (14), 5119–5123.
- (66) Hesari, M.; Ding, Z. Spooling electrochemiluminescence spectroscopy: development, applications and beyond. *Nat. Protoc.* **2021**, *16* (4), 2109–2130.
- (67) Fereja, T. H.; Du, F.; Wang, C.; Snizhko, D.; Guan, Y.; Xu, G. Electrochemiluminescence Imaging Techniques for Analysis and Visualizing. *J. Anal. Test.* **2020**, *4* (2), 76–91.
- (68) Ma, C.; Wei, H.-F.; Wang, M.-X.; Wu, S.; Chang, Y.-C.; Zhang, J.; Jiang, L.-P.; Zhu, W.; Chen, Z.; Lin, Y. Hydrogen Evolution Reaction Monitored by Electrochemiluminescence Blinking at Single-Nanoparticle Level. *Nano Lett.* **2020**, *20* (7), 5008–5016.
- (69) Chen, M.-M.; Xu, C.-H.; Zhao, W.; Chen, H.-Y.; Xu, J.-J. Observing the structure-dependent electrocatalytic activity of bimetallic Pd-Au nanorods at the single-particle level. *Chem. Commun.* **2020**, *56* (23), 3413–3416.
- (70) Sentic, M.; Milutinovic, M.; Kanoufi, F.; Manojlovic, D.; Arbault, S.; Sojic, N. Mapping electrogenerated chemiluminescence reactivity in space: mechanistic insight into model systems used in immunoassays. *Chem. Sci.* **2014**, *5* (6), 2568–2572.
- (71) Chen, Y.; Zhou, S.; Li, L.; Zhu, J.-j. Nanomaterials-based sensitive electrochemiluminescence biosensing. *Nano Today* **2017**, *12*, 98–115.
- (72) Li, L.; Chen, Y.; Zhu, J.-J. Recent Advances in Electrochemiluminescence Analysis. *Anal. Chem.* **2017**, *89* (1), 358–371.
- (73) Wen, W.; Yan, X.; Zhu, C.; Du, D.; Lin, Y. Recent Advances in Electrochemical Immunosensors. *Anal. Chem.* **2017**, *89* (1), 138–156.
- (74) Chovin, A.; Garrigue, P.; Sojic, N. Electrochemiluminescent detection of hydrogen peroxide with an imaging sensor array. *Electrochim. Acta* **2004**, *49* (22-23), 3751–3757.
- (75) Chovin, A.; Garrigue, P.; Sojic, N. Remote NADH imaging through an ordered array of electrochemiluminescent nanoapertures. *Bioelectrochemistry* **2006**, *69* (1), 25–33.
- (76) Ding, J.; Zhou, P.; Guo, W.; Su, B. Confined Electrochemiluminescence Generation at Ultra-High-Density Gold Micro-

well Electrodes. *Front. Chem.* **2021**, *8*, DOI: 10.3389/fchem.2020.630246.

(77) Fiorani, A.; Han, D.; Jiang, D.; Fang, D.; Paolucci, F.; Sojic, N.; Valenti, G. Spatially resolved electrochemiluminescence through a chemical lens. *Chem. Sci.* **2020**, *11* (38), 10496–10500.

(78) Zanut, A.; Fiorani, A.; Canola, S.; Saito, T.; Ziebart, N.; Rapino, S.; Rebecani, S.; Barbon, A.; Irie, T.; Josel, H. P.; Negri, F.; Marcaccio, M.; Windfuhr, M.; Imai, K.; Valenti, G.; Paolucci, F. Insights into the mechanism of coreactant electrochemiluminescence facilitating enhanced bioanalytical performance. *Nat. Commun.* **2020**, *11*, 2668.

(79) Valenti, G.; Scarabino, S.; Goudeau, B.; Lesch, A.; Jovic, M.; Villani, E.; Sentic, M.; Rapino, S.; Arbault, S.; Paolucci, F.; Sojic, N. Single Cell Electrochemiluminescence Imaging: From the Proof-of-Concept to Disposable Device-Based Analysis. *J. Am. Chem. Soc.* **2017**, *139* (46), 16830–16837.

(80) Szunerits, S.; Tam, J. M.; Thouin, L.; Amatore, C.; Walt, D. R. Spatially resolved electrochemiluminescence on an array of electrode tips. *Anal. Chem.* **2003**, *75* (17), 4382–4388.

(81) Sentic, M.; Virgilio, F.; Zanut, A.; Manojlovic, D.; Arbault, S.; Tormen, M.; Sojic, N.; Ugo, P. Microscopic imaging and tuning of electrogenerated chemiluminescence with boron-doped diamond nanoelectrode arrays. *Anal. Bioanal. Chem.* **2016**, *408* (25), 7085–7094.

(82) Zhang, J.; Zhou, J.; Tian, C.; Yang, S.; Jiang, D.; Zhang, X. X.; Chen, H. Y. Localized Electrochemiluminescence from Nanoneedle Electrodes for Very-High-Density Electrochemical Sensing. *Anal. Chem.* **2017**, *89* (21), 11399–11404.

(83) Wang, N.; Ao, H.; Xiao, W.; Chen, W.; Li, G.; Wu, J.; Ju, H. Confined electrochemiluminescence imaging microarray for high-throughput biosensing of single cell-released dopamine. *Biosens. Bioelectron.* **2022**, *201*, 113959.

(84) Wang, N.; Chen, L.; Chen, W.; Ju, H. Potential- and Color-Resolved Electrochemiluminescence of Polymer Dots for Array Imaging of Multiplex MicroRNAs. *Anal. Chem.* **2021**, *93* (12), 5327–5333.

(85) Deiss, F.; LaFratta, C. N.; Symer, M.; Blicharz, T. M.; Sojic, N.; Walt, D. R. Multiplexed Sandwich Immunoassays Using Electrochemiluminescence Imaging Resolved at the Single Bead Level. *J. Am. Chem. Soc.* **2009**, *131* (17), 6088–6089.

(86) Guo, W.; Ding, H.; Gu, C.; Liu, Y.; Jiang, X.; Su, B.; Shao, Y. Potential-Resolved Multicolor Electrochemiluminescence for Multiplex Immunoassay in a Single Sample. *J. Am. Chem. Soc.* **2018**, *140* (46), 15904–15915.

(87) Wang, Z.; Gao, H.; Liu, P.; Wu, X.; Li, Q.; Xu, J.-J.; Hua, D. Visualized uranium rapid monitoring system based on self-enhanced electrochemiluminescence-imaging of amidoxime functionalized polymer nanoparticles. *Chin. Chem. Lett.* **2022**, *33* (7), 3456–3460.

(88) Zanut, A.; Palomba, F.; Rossi Scota, M.; Rebecani, S.; Marcaccio, M.; Genovese, D.; Rampazzo, E.; Valenti, G.; Paolucci, F.; Prodi, L. Dye-Doped Silica Nanoparticles for Enhanced ECL-Based Immunoassay Analytical Performance. *Angew. Chem. Int. Ed.* **2020**, *59* (49), 21858–21863.

(89) Rebecani, S.; Wetzl, C.; Zamolo, V. A.; Criado, A.; Valenti, G.; Paolucci, F.; Prato, M. Electrochemiluminescent immunoassay enhancement driven by carbon nanotubes. *Chem. Commun. (Camb)* **2021**, *57* (76), 9672–9675.

(90) Han, D.; Goudeau, B.; Lapeyre, V.; Ravaine, V.; Jiang, D.; Fang, D.; Sojic, N. Enhanced electrochemiluminescence at microgel-functionalized beads. *Biosens. Bioelectron.* **2022**, *216*, 114640–114640.

(91) Ismail, A.; Voci, S.; Descamps, L.; Buhot, A.; Sojic, N.; Leroy, L.; Bouchet-Spinelli, A. Bipolar Electrochemiluminescence Imaging: A Way to Investigate the Passivation of Silicon Surfaces. *ChemPhysChem* **2021**, *22* (11), 1094–1100.

(92) Sentic, M.; Arbault, S.; Goudeau, B.; Manojlovic, D.; Kuhn, A.; Bouffier, L.; Sojic, N. Electrochemiluminescent swimmers for dynamic enzymatic sensing. *Chem. Commun. (Camb)* **2014**, *50* (71), 10202–5.

(93) Sentic, M.; Loget, G.; Manojlovic, D.; Kuhn, A.; Sojic, N. Light-Emitting Electrochemical "Swimmers". *Angew. Chem. Int. Ed.* **2012**, *51* (45), 11284–11288.

(94) Chow, K. F.; Mavre, F.; Crooks, R. M. Wireless electrochemical DNA microarray sensor. *J. Am. Chem. Soc.* **2008**, *130* (24), 7544–5.

(95) Zhang, J.-D.; Yu, T.; Li, J.-Y.; Xu, J.-J.; Chen, H.-Y. An ITO bipolar array for electrochemiluminescence imaging of H₂O₂. *Electrochem. Commun.* **2014**, *49*, 75–78.

(96) Wu, S.; Zhou, Z.; Xu, L.; Su, B.; Fang, Q. Integrating bipolar electrochemistry and electrochemiluminescence imaging with microdroplets for chemical analysis. *Biosens. Bioelectron.* **2014**, *53*, 148–153.

(97) Wang, Y.-Z.; Zhao, W.; Dai, P.-P.; Lu, H.-J.; Xu, J.-J.; Pan, J.; Chen, H.-Y. Spatial-resolved electrochemiluminescence ratiometry based on bipolar electrode for bioanalysis. *Biosens. Bioelectron.* **2016**, *86*, 683–689.

(98) Dutta, P.; Han, D.; Goudeau, B.; Jiang, D.; Fang, D.; Sojic, N. Reactivity mapping of luminescence in space: Insights into heterogeneous electrochemiluminescence bioassays. *Biosens. Bioelectron.* **2020**, *165*, 112372.

(99) Chang, Y.-L.; Palacios, R. E.; Fan, F.-R. F.; Bard, A. J.; Barbara, P. F. Electrogenerated Chemiluminescence of Single Conjugated Polymer Nanoparticles. *J. Am. Chem. Soc.* **2008**, *130* (28), 8906–8907.

(100) Wilson, A. J.; Marchuk, K.; Willets, K. A. Imaging Electrogenerated Chemiluminescence at Single Gold Nanowire Electrodes. *Nano Lett.* **2015**, *15* (9), 6110–6115.

(101) Pan, S.; Liu, J.; Hill, C. M. Observation of Local Redox Events at Individual Au Nanoparticles Using Electrogenerated Chemiluminescence Microscopy. *J. Phys. Chem. C* **2015**, *119* (48), 27095–27103.

(102) Chen, M. M.; Zhao, W.; Zhu, M. J.; Li, X. L.; Xu, C. H.; Chen, H. Y.; Xu, J. J. Spatiotemporal imaging of electrocatalytic activity on single 2D gold nanoplates via electrogenerated chemiluminescence microscopy. *Chem. Sci.* **2019**, *10* (15), 4141–4147.

(103) Zhu, M. J.; Pan, J. B.; Wu, Z. Q.; Gao, X. Y.; Zhao, W.; Xia, X. H.; Xu, J. J.; Chen, H. Y. Electrogenerated Chemiluminescence Imaging of Electrocatalysis at a Single Au-Pt Janus Nanoparticle. *Angew. Chem. Int. Ed. Engl.* **2018**, *57* (15), 4010–4014.

(104) Zhu, H.; Jiang, D.; Zhu, J.-J. High-resolution imaging of catalytic activity of a single graphene sheet using electrochemiluminescence microscopy. *Chem. Sci.* **2021**, *12* (13), 4794–4799.

(105) Zhu, H.; Jin, R.; Jiang, D.; Zhu, J. J. Perturbation Electrochemiluminescence Imaging to Observe the Fluctuation of Charge-Transfer Resistance in Individual Graphene Microsheets with Redox-Induced Defects. *ACS Appl. Mater. Interfaces* **2019**, *11* (50), 46666–46670.

(106) Zhu, H.; Jin, R.; Chang, Y. C.; Zhu, J. J.; Jiang, D.; Lin, Y.; Zhu, W. Understanding the Synergistic Oxidation in Dichalcogenides through Electrochemiluminescence Blinking at Millisecond Resolution. *Adv. Mater.* **2021**, *33* (48), 2105039.

(107) Chen, Y.; Fu, J.; Cui, C.; Jiang, D.; Chen, Z.; Chen, H.-Y.; Zhu, J.-J. In Situ Visualization of Electrocatalytic Reaction Activity at Quantum Dots for Water Oxidation. *Anal. Chem.* **2018**, *90* (14), 8635–8641.

(108) Chen, Y.; Zhao, D.; Fu, J.; Gou, X.; Jiang, D.; Dong, H.; Zhu, J. J. In Situ Imaging Facet-Induced Spatial Heterogeneity of Electrocatalytic Reaction Activity at the Subparticle Level via Electrochemiluminescence Microscopy. *Anal. Chem.* **2019**, *91* (10), 6829–6835.

(109) Guo, W.; Ding, H.; Zhou, P.; Wang, Y.; Su, B. Electrochemiluminescence Waveguide in Single Crystalline Molecular Wires. *Angew. Chem. Int. Ed.* **2020**, *59* (17), 6745–6749.

(110) Wang, N.; Gao, H.; Li, Y.; Li, G.; Chen, W.; Jin, Z.; Lei, J.; Wei, Q.; Ju, H. Dual Intramolecular Electron Transfer for In Situ Coreactant-Embedded Electrochemiluminescence Microimaging of Membrane Protein. *Angew. Chem. Int. Ed.* **2021**, *60* (1), 197–201.

(111) Liu, G.; Jin, B.-K.; Ma, C.; Chen, Z.; Zhu, J.-J. Potential-Resolved Electrochemiluminescence Nanoprobes for Visual Apoptosis

- Evaluation at Single-Cell Level. *Anal. Chem.* **2019**, *91* (9), 6363–6370.
- (112) Liu, Y.; Zhang, H.; Li, B.; Liu, J.; Jiang, D.; Liu, B.; Sojic, N. Single Biomolecule Imaging by Electrochemiluminescence. *J. Am. Chem. Soc.* **2021**, *143* (43), 17910–17914.
- (113) Cao, J.-T.; Wang, Y.-L.; Zhang, J.-J.; Dong, Y.-X.; Liu, F.-R.; Ren, S.-W.; Liu, Y.-M. Immuno-Electrochemiluminescent Imaging of a Single Cell Based on Functional Nanoprobes of Heterogeneous Ru(bpy)₃(2+)₂@SiO₂/Au Nanoparticles. *Anal. Chem.* **2018**, *90* (17), 10334–10339.
- (114) Li, B.; Huang, X.; Lu, Y.; Fan, Z.; Li, B.; Jiang, D.; Sojic, N.; Liu, B. High Electrochemiluminescence from Ru(bpy)₃(2+) Embedded Metal-Organic Frameworks to Visualize Single Molecule Movement at the Cellular Membrane. *Adv. Sci. (Weinh)* **2022**, *9*, 2204715.
- (115) Ma, C.; Wu, S.; Zhou, Y.; Wei, H. F.; Zhang, J.; Chen, Z.; Zhu, J. J.; Lin, Y.; Zhu, W. Bio-Coreactant-Enhanced Electrochemiluminescence Microscopy of Intracellular Structure and Transport. *Angew. Chem. Int. Ed. Engl.* **2021**, *60* (9), 4907–4914.
- (116) Chen, Y.; Gou, X.; Ma, C.; Jiang, D.; Zhu, J.-J. A Synergistic Coreactant for Single-Cell Electrochemiluminescence Imaging: Guanine-Rich ssDNA-Loaded High-Index Faceted Gold Nanoflowers. *Anal. Chem.* **2021**, *93* (21), 7682–7689.
- (117) Zhou, J.; Ma, G.; Chen, Y.; Fang, D.; Jiang, D.; Chen, H.-y. Electrochemiluminescence Imaging for Parallel Single-Cell Analysis of Active Membrane Cholesterol. *Anal. Chem.* **2015**, *87* (16), 8138–8143.
- (118) Zhang, J.; Ding, H.; Zhao, S.; Jiang, D.; Chen, H.-Y. Confined electrochemiluminescence in vertically ordered silica mesochannels for the imaging of hydrogen peroxide released from single cells. *Electrochem. Commun.* **2019**, *98*, 38–42.
- (119) Liu, G.; Ma, C.; Jin, B.-K.; Chen, Z.; Zhu, J.-J. Direct Electrochemiluminescence Imaging of a Single Cell on a Chitosan Film Modified Electrode. *Anal. Chem.* **2018**, *90* (7), 4801–4806.
- (120) Li, X.; Qin, X.; Wang, Z.; Wu, Y.; Wang, K.; Xia, X.; Liu, S. In Situ Imaging of Endogenous Hydrogen Peroxide Efflux from Living Cells via Bipolar Gold Nanoelectrode Array and Electrochemiluminescence Technology. *ACS Sensors* **2022**, *7* (8), 2446–2453.
- (121) Cui, C.; Chen, Y.; Jiang, D.; Chen, H.-Y.; Zhang, J.; Zhu, J.-J. Steady-State Electrochemiluminescence at Single Senniconductive Titanium Dioxide Nanoparticles for Local Sensing of Single Cells. *Anal. Chem.* **2019**, *91* (1), 1121–1125.
- (122) Zhang, J.; Jin, R.; Chen, Y.; Fang, D.; Jiang, D. Enhanced electrochemiluminescence at single lithium iron phosphate nanoparticles for the local sensing of hydrogen peroxide efflux from single living cell under a low voltage. *Sens. Actuators, B* **2021**, *329*, 129208.
- (123) Gao, W.; Liu, Y.; Zhang, H.; Wang, Z. Electrochemiluminescence Biosensor for Nucleolin Imaging in a Single Tumor Cell Combined with Synergetic Therapy of Tumor. *Acs Sensors* **2020**, *5* (4), 1216–1222.
- (124) Hiramoto, K.; Ino, K.; Komatsu, K.; Nashimoto, Y.; Shiku, H. Electrochemiluminescence imaging of respiratory activity of cellular spheroids using sequential potential steps. *Biosens. Bioelectron.* **2021**, *181*, 113123.
- (125) Ding, L.; Ding, H.; Zhou, P.; Xi, L.; Su, B. Surface-Sensitive Imaging Analysis of Cell-Microenvironment Interactions by Electrochemiluminescence Microscopy. *Anal. Chem.* **2022**, *94* (30), 10885–10892.
- (126) Gao, H.; Han, W.; Qi, H.; Gao, Q.; Zhang, C. Electrochemiluminescence Imaging for the Morphological and Quantitative Analysis of Living Cells under External Stimulation. *Anal. Chem.* **2020**, *92* (12), 8278–8284.
- (127) Chen, M.-M.; Xu, C.-H.; Zhao, W.; Chen, H.-Y.; Xu, J.-J. Single Cell Imaging of Electrochemiluminescence-Driven Photodynamic Therapy. *Angew. Chem. Int. Ed.* **2022**, *61* (16), e202117401.
- (128) Ino, K.; Komatsu, K.; Hiramoto, K.; Utagawa, Y.; Nashimoto, Y.; Shiku, H. Electrochemiluminescence imaging of cellular adhesion in vascular endothelial cells during tube formation on hydrogel scaffolds. *Electrochim. Acta* **2022**, *415*, 140240.
- (129) Ma, C.; Xing, Z.; Gou, X.; Jiang, L.-P.; Zhu, J.-J. A temperature-tuned electrochemiluminescence layer for reversibly imaging cell topography. *Chem. Sci.* **2022**, *13*, 13938–13947.
- (130) Xu, J.; Huang, P.; Qin, Y.; Jiang, D.; Chen, H.-y. Analysis of Intracellular Glucose at Single Cells Using Electrochemiluminescence Imaging. *Anal. Chem.* **2016**, *88* (9), 4609–4612.
- (131) Xia, J.; Zhou, J.; Zhang, R.; Jiang, D.; Jiang, D. Gold-coated polydimethylsiloxane microwells for high-throughput electrochemiluminescence analysis of intracellular glucose at single cells. *Anal. Bioanal. Chem.* **2018**, *410* (20), 4787–4792.
- (132) Loget, G.; Roche, J.; Kuhn, A. True Bulk Synthesis of Janus Objects by Bipolar Electrochemistry. *Adv. Mater.* **2012**, *24* (37), 5111–5116.
- (133) Gao, R.; Lin, Y.; Ying, Y.-L.; Hu, Y.-X.; Xu, S.-W.; Ruan, L.-Q.; Yu, R.-J.; Li, Y.-J.; Li, H.-W.; Cui, L.-F.; Long, Y.-T. Wireless nanopore electrodes for analysis of single entities. *Nature Protoc* **2019**, *14* (7), 2015–2035.
- (134) McKelvey, K.; Perry, D.; Byers, J. C.; Colburn, A. W.; Unwin, P. R. Bias Modulated Scanning Ion Conductance Microscopy. *Anal. Chem.* **2014**, *86* (7), 3639–3646.
- (135) Ying, Y.-L.; Hu, Y.-X.; Gao, R.; Yu, R.-J.; Gu, Z.; Lee, L. P.; Long, Y.-T. Asymmetric Nanopore Electrode-Based Amplification for Electron Transfer Imaging in Live Cells. *J. Am. Chem. Soc.* **2018**, *140* (16), 5385–5392.
- (136) He, R.; Tang, H.; Jiang, D.; Chen, H.-y. Electrochemical Visualization of Intracellular Hydrogen Peroxide at Single Cells. *Anal. Chem.* **2016**, *88* (4), 2006–2009.
- (137) Wang, Y.; Jin, R.; Sojic, N.; Jiang, D.; Chen, H. Y. Intracellular Wireless Analysis of Single Cells by Bipolar Electrochemiluminescence Confined in a Nanopipette. *Angew. Chem. Int. Ed. Engl.* **2020**, *59* (26), 10416–10420.
- (138) Zhang, J.; Jin, R.; Jiang, D.; Chen, H.-Y. Electrochemiluminescence-Based Capacitance Microscopy for Label-Free Imaging of Antigens on the Cellular Plasma Membrane. *J. Am. Chem. Soc.* **2019**, *141* (26), 10294–10299.
- (139) Wang, Y.; Guo, W.; Yang, Q.; Su, B. Electrochemiluminescence Self-Interference Spectroscopy with Vertical Nanoscale Resolution. *J. Am. Chem. Soc.* **2020**, *142* (3), 1222–1226.
- (140) Han, D.; Goudeau, B.; Manojlovic, D.; Jiang, D.; Fang, D.; Sojic, N. Electrochemiluminescence Loss in Photobleaching. *Angew. Chem. Int. Ed.* **2021**, *60* (14), 7686–7690.
- (141) Dong, J.; Xu, Y.; Zhang, Z.; Feng, J. Operando Imaging of Chemical Activity on Gold Plates with Single-Molecule Electrochemiluminescence Microscopy. *Angew. Chem. Int. Ed.* **2022**, *61* (14), e202200187.
- (142) Tan, J.; Xu, L.; Li, T.; Su, B.; Wu, J. Image-Contrast Technology Based on the Electrochemiluminescence of Porous Silicon and Its Application in Fingerprint Visualization. *Angew. Chem. Int. Ed.* **2014**, *53* (37), 9822–9826.
- (143) Xu, L.; Li, Y.; Wu, S.; Liu, X.; Su, B. Imaging Latent Fingerprints by Electrochemiluminescence. *Angew. Chem. Int. Ed.* **2012**, *51* (32), 8068–8072.